

Summer 2008

Application of Kalman Filtering to Real-time Flight Regime Recognition Algorithms in a Helicopter Health and Usage Monitoring System

Rachel Elizabeth Rajnicek
Embry-Riddle Aeronautical University - Daytona Beach

Follow this and additional works at: <https://commons.erau.edu/db-theses>



Part of the [Aerospace Engineering Commons](#), and the [Aviation Commons](#)

Scholarly Commons Citation

Rajnicek, Rachel Elizabeth, "Application of Kalman Filtering to Real-time Flight Regime Recognition Algorithms in a Helicopter Health and Usage Monitoring System" (2008). *Theses - Daytona Beach*. 169. <https://commons.erau.edu/db-theses/169>

This thesis is brought to you for free and open access by Embry-Riddle Aeronautical University – Daytona Beach at ERAU Scholarly Commons. It has been accepted for inclusion in the Theses - Daytona Beach collection by an authorized administrator of ERAU Scholarly Commons. For more information, please contact commons@erau.edu.

APPLICATION OF KALMAN FILTERING TO REAL-TIME
FLIGHT REGIME RECOGNITION ALGORITHMS IN A
HELICOPTER HEALTH AND USAGE MONITORING SYSTEM

by

Rachel Elizabeth Rajnicek

A Thesis Submitted to the
Graduate Studies Office
In Partial Fulfillment of the Requirements for the
Degree of Master of Science in Aerospace Engineering

Embry-Riddle Aeronautical University
Daytona Beach, Florida
Summer 2008

UMI Number: EP32030

INFORMATION TO USERS

The quality of this reproduction is dependent upon the quality of the copy submitted. Broken or indistinct print, colored or poor quality illustrations and photographs, print bleed-through, substandard margins, and improper alignment can adversely affect reproduction.

In the unlikely event that the author did not send a complete manuscript and there are missing pages, these will be noted. Also, if unauthorized copyright material had to be removed, a note will indicate the deletion.

UMI[®]

UMI Microform EP32030
Copyright 2011 by ProQuest LLC
All rights reserved. This microform edition is protected against
unauthorized copying under Title 17, United States Code.

ProQuest LLC
789 East Eisenhower Parkway
P.O. Box 1346
Ann Arbor, MI 48106-1346

Copyright by Rachel Elizabeth Rajnicek 2008

All Rights Reserved

APPLICATION OF KALMAN FILTERING TO REAL-TIME FLIGHT REGIME RECOGNITION
ALGORITHMS IN A HELICOPTER HEALTH AND USAGE MONITORING SYSTEM

by

Rachel Elizabeth Rajnicek

This thesis was prepared under the direction of the candidate's thesis committee chairman, Dr. Richard "Pat" Anderson, Department of Aerospace Engineering, and has been approved by the members of her thesis committee. It was submitted to the Department of Aerospace Engineering and was accepted in partial fulfillment of the requirements for the degree of Master of Science in Aerospace Engineering.

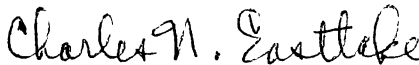
THESIS COMMITTEE:



Dr. Richard "Pat" Anderson
Chairman

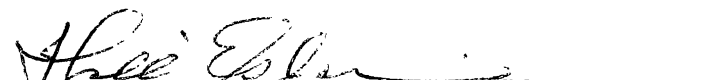


Dr. Nickolas "Dan" Macchiarella
Member



Professor Charles Eastlake
Member

Coordinator, MSAE Program



Department Chair, Aerospace Engineering

7/31/08
Date



Associate Provost

7-31-08
Date

ACKNOWLEDGEMENTS

This thesis is the culmination of three years work on the HUMS project and two years work on my Master's degree. "And when you want something, all the universe conspires in helping you to achieve it" Paulo Coelho The Alchemist. I would not have gotten to this point without the help, love, and support of many people.

I would like to thank Dr. Macchiarella and Prof. Eastlake for participating on my thesis committee and their stories/insights about helicopters. Thank you to Dr. Richard "Pat" Anderson for asking me to work on the HUMS project, helping me figure out a thesis topic, and truly appreciating the research outputs from this thesis. I would not be a Flight Test Engineer without the experience gained from the HUMS project. I would like to thank my coworkers and friends from the Applied Engineering Research Center. Monica Londono, who helped double-check my math, endlessly discussing matrices, and was patient when I filled the office with whiteboards of equations. Whenever I felt like this thesis would never end, you made me laugh. Christopher R. Brown, the code would not work as well as it does without your knowledge and help with Matlab. Dik, the movies would not work, nor would the real-time display have labels without your help. Thank you to the many other students and faculty at ERAU who inspired or supported my research and studies.

I also want to thank my friends and family for all their love and support. Jen, I would go crazy if you did not smile and nod when I talk engineering around you and if you never reminded me to stop and listen to the bassist. Amber, on the worst days you were always there to give me a lift and keep me going. Chris, Robert, and Pat you are the most exasperating brothers but you are also supportive and sometimes understand when I talk engineer. Most importantly, I want to thank my parents who have never stopped believing that I CAN do anything. Your unwavering love and support has contributed immensely to my achieving this degree and finishing this thesis.

ABSTRACT

Author: Rachel Elizabeth Rajnicek
Title: Application of Kalman Filtering to Real-time Flight Regime Recognition Algorithms in a Helicopter Health and Usage Monitoring System
Institution: Embry-Riddle Aeronautical University
Degree: Master of Science in Aerospace Engineering
Year: 2007-2008

The purpose of this study is the application of Kalman filters to real-time Flight Regime Recognition (FRR) algorithms to identify the regime flown and observe transitions between flight regimes. Rotor fault identification, a technique that is somewhat similar to flight regime recognition, successfully used Kalman filters to determine fault types and damage locations. Recently developed FRR algorithms successfully applied Hidden Markov Models, which are similar to Kalman filters. The selected regime set for this study derives from a study performed by Bell Helicopter Textron, Inc. The selected parameter set for this study is modified from the Schweizer 300 Flight Test Program performed by Embry-Riddle Aeronautical University. The FRR algorithms developed will use the recorded flight parameters to identify a flight regime. A graphical interface allows the user to observe the real-time FRR and transitions between regimes. This research aims to bridge the gap between the application of mathematical models for damage identification and regime recognition. Multiple mathematical models developed for rotor blade fault and damage identification include neural networks, fuzzy logic systems, and Kalman filters. Recent research indicates that only the neural network approach has been applied to FRR algorithms, and that a Hidden Markov Model (HMM) approach outperformed the neural network. Additionally, public domain regime recognition research focuses on post processing algorithms rather than real-time regime recognition. The post processing codes appear to use discrete algorithms, which do not clearly identify transitions between regimes.

TABLE OF CONTENTS

| | |
|---|------|
| ACKNOWLEDGEMENTS | iv |
| ABSTRACT | v |
| LIST OF FIGURES | viii |
| LIST OF ACRONYMS | ix |
| NOMENCLATURE | x |
| 1. INTRODUCTION | 1 |
| 1.1 HUMS Background | 1 |
| 1.2 Flight Regime Recognition Background..... | 2 |
| 1.3 Kalman Filtering Background..... | 2 |
| 2. SCOPE AND APPLICABILITY | 4 |
| 2.1 Motivation for Research..... | 4 |
| 2.2 Problem Statement | 4 |
| 2.3 Review of Related Literature..... | 5 |
| 2.4 Hypothesis..... | 8 |
| 3. METHODS | 9 |
| 3.1 Design and Instrumentation..... | 9 |
| 3.2 Data Analysis | 9 |
| 4. PROCEDURE..... | 10 |
| 4.1 General Differential Equations for Zero Order Polynomial..... | 10 |
| 4.2 General Equations for a Discrete Kalman Filter | 10 |
| 4.3 General Discrete Kalman Filter for FRR..... | 11 |
| 4.4 Flow Chart of Discrete FRR Kalman Filter Equations..... | 14 |
| 4.5 Sample Kalman Filter for FRR..... | 17 |

| | | |
|-------|--|----|
| 4.5.1 | Inputs..... | 17 |
| 4.5.2 | Outputs..... | 20 |
| 4.5.3 | Sample Data | 20 |
| 5. | ANALYSIS | 22 |
| 5.1 | Real-Time FRR via Display..... | 22 |
| 5.1.1 | Single Regime Identification..... | 22 |
| 5.1.2 | Combination Maneuver Identification | 25 |
| 5.2 | Post Processing Regime Specific FRR | 27 |
| 5.2.1 | On Ground | 28 |
| 5.2.2 | High Speed..... | 32 |
| 5.2.3 | Low Speed | 33 |
| 5.2.4 | Right Turn | 34 |
| 5.2.5 | Left Turn | 35 |
| 5.2.6 | Climb..... | 36 |
| 5.2.7 | Descend | 37 |
| 5.2.8 | Steady/Level Flight | 38 |
| 5.3 | Post Processing Regime Transition Identification | 40 |
| 5.4 | Variation of Process Noise..... | 41 |
| 6. | CONCLUSIONS | 45 |
| 7. | REFERENCES | 47 |
| 8. | APPENDIX A: Identified Regimes | 49 |
| 9. | APPENDIX B: Flight Parameters..... | 50 |

LIST OF FIGURES

| | |
|---|----|
| Figure 1: Flowchart of Equations for FRR Kalman Filter..... | 15 |
| Figure 2: Screenshot of FRR Algorithm Model Top Level..... | 16 |
| Figure 3: Screenshot of FRR Kalman Filter Top Level..... | 16 |
| Figure 4: Sample FRR Identification | 21 |
| Figure 5: Real-Time On Ground Recognition..... | 23 |
| Figure 6: Real-Time High Speed Level Recognition..... | 24 |
| Figure 7: Real-Time Low Speed Level Recognition..... | 25 |
| Figure 8: Real-Time High Speed Climb Recognition | 26 |
| Figure 9: Real-Time High Speed Climbing Right Turn Recognition..... | 27 |
| Figure 10: Sample FRR Graph..... | 28 |
| Figure 11: On Ground Identification | 29 |
| Figure 12: Running Landing Identification | 30 |
| Figure 13: Autorotation Identification | 31 |
| Figure 14: High Speed Identification..... | 32 |
| Figure 15: Low Speed Identification..... | 33 |
| Figure 16: Right Turn Identification..... | 34 |
| Figure 17: Left Turn Identification..... | 35 |
| Figure 18: Climb Identification | 37 |
| Figure 19: Descend Identification | 38 |
| Figure 20: Steady/Level Flight Identification..... | 39 |
| Figure 21: Regime Transitions | 40 |
| Figure 22: Regime Transitions with $Q_k = 1$ | 41 |
| Figure 23: Regime Transitions with $Q_k = 0.00001$ | 42 |
| Figure 24: Regime Transitions with $Q_k = 0.01$ | 42 |
| Figure 25: Regime Identification with $Q_k = 0.0005$ | 43 |

LIST OF ACRONYMS

| | |
|---------|--------------------------------------|
| AC | Advisory Circular |
| COTS | Commercial off the Shelf |
| DESCD | Descend |
| ELL ALT | Ellipsoidal Altitude |
| ERAU | Embry-Riddle Aeronautical University |
| FAA | Federal Aviation Administration |
| FRR | Flight Regime Recognition |
| HMM | Hidden Markov Model |
| HISPD | High Speed |
| HUMS | Health and Usage Monitoring System |
| IAS | Indicated Air Speed |
| INV | Inverse |
| LOSPD | Low Speed |
| LTurn | Left Turn |
| LVL | Level |
| MG | Miscellaneous Guidance |
| OEM | Original Equipment Manufacturer |
| OnGnd | On Ground |
| PC | Personal Computer |
| RCDT | Rotorcraft Damage Tolerance |
| ROC | Rate of Climb |
| RTurn | Right Turn |
| WOW | Weight on Wheels |

NOMENCLATURE

| | | |
|---------------------|---|-------------------------------------|
| x | = | State Estimate |
| a_0 | = | Constant |
| \dot{x} | = | First Derivative of x |
| F | = | System Dynamics Matrix |
| w | = | Random Forcing Function |
| z_k | = | Measurement Vector |
| H | = | Connection Matrix |
| x_k | = | Performance Index Updated |
| v_k | = | Measurement Noise |
| \hat{x}_k | = | Estimated Updated Performance Index |
| Φ_k | = | State Transition Matrix |
| \hat{x}_{k-1} | = | Estimated Current Performance Index |
| w_k | = | Process Noise |
| K_k | = | Kalman Gain |
| M_k | = | Updated Covariance Matrix |
| P_{k-1} | = | Current Covariance Matrix |
| Q_k | = | Estimated Process Noise |
| R_k | = | Signal Variance Matrix |
| $P_{k_{int}}$ | = | Initial Covariance Matrix Estimate |
| $\hat{x}_{k_{int}}$ | = | Initial Performance Index Estimate |
| I | = | Identity Matrix |

1. INTRODUCTION

The Federal Aviation Administration (FAA) Aging Aircraft Directorate currently oversees Rotorcraft Structural Integrity and Safety research. This research focuses on two areas: Rotorcraft Damage Tolerance (RCDT) and Helicopter Health and Usage Monitoring Systems (HUMS). Desired outcomes of RCDT research include developing technologies and data to reduce rotorcraft structural failures. Desired outcomes of HUMS research include validating Advisory Circular (AC) 29-2C Miscellaneous Guidance (MG) 15 for HUMS installation and maintenance credits [1]. The *HUMS Research and Development Roadmap – 10 Year Plan* outlines the FAA plan for HUMS research from 2005 through 2015. The roadmap also identifies Flight Regime Recognition (FRR) as a key component of HUMS Research. The HUMS roadmap requires FRR research in the following areas: HUMS AC Requirement Compliance Demonstration, HUMS Development and Equipped-Flight Testing, and Structural Usage Monitoring and Credit Validation [2].

1.1 HUMS Background

A helicopter Health and Usage Monitoring System (HUMS) is a system of hardware and software which records and analyzes flight parameters either for real-time mitigation (health monitoring) or post-processing (usage monitoring). The HUMS health monitoring functionality can alert pilots to impending component failures or excessively damaging flight maneuvers. Impending component failures can include blade crack propagation or pitting on transmission gears. Excessively damaging flight maneuvers can produce abnormally high g-loads on the airframe or cause abnormally high stresses throughout flight critical components. Once the pilot receives an alert to impending component failure or an excessively damaging flight maneuver, the rotorcraft can land as soon as practical or the maneuver ended. This is a real-time mitigation because the after the in-flight alert pilot immediately takes action to eliminate or minimize failure of the rotorcraft.

In contrast, the HUMS usage monitoring functionality allows owner/operators to monitor a rotorcraft's actual usage spectrum. The actual usage spectrum can justify

maintenance credits or early part replacement. An owner/operator achieves maintenance credits when the actual usage spectrum is less damaging than the certification spectrum for a life-limited component. Maintenance credits include eliminating hourly inspections or extending the service life of a life-limited component beyond the replacement or overhaul time published by the manufacturer. Maintenance credits are desirable for owner/operators as they can reduce the overall maintenance cost for a rotorcraft. Early part replacement can be required when a rotorcraft's actual usage spectrum is more damaging than its certification spectrum. In this situation, a life-limited component must be overhauled or replaced prior to the manufacturer's published life-limit. Early part replacement is desirable to reduce component failures that could result in accidents or fatalities. Ultimately, early part replacement based upon an actual usage spectrum can increase the safety and reliability of rotorcraft.

A typical HUMS consists of an onboard data acquisition unit, onboard sensors, and a ground station used for data processing and analysis. The end-to-end HUMS consists of all the hardware and software used in both the airborne and ground stations to acquire, store, process, and analyze the HUMS data.

1.2 Flight Regime Recognition Background

The end-to-end HUMS includes data analysis tools such as Flight Regime Recognition (FRR) algorithms. FRR algorithms determine the rotorcraft's flight profile maneuver using the recorded flight data. Examples of flight profile maneuvers include 65kt level flight and $>60^\circ$ banked ascending right turn. FRR analysis transpires either in real-time by the onboard portion of the HUMS or during post processing by the ground based portion of the HUMS. FRR data analysis aids in generating the actual usage spectrum. FRR algorithms employ mathematical decision-making to determine the current flight regime. The mathematical basis for the flight regime recognition developed in this study is Kalman filtering.

1.3 Kalman Filtering Background

A Kalman Filter is a recursive filter that can estimate the state of a system from noisy measurements. A set of linear differential equations must describe the system. The state is a variable that completely specifies the status of the system at any given time [3]. The Kalman

filter is recursive because it uses state feedback to determine the state estimate at the next time step. The Kalman filtering technique has been readily utilized since R. E. Kalman published his filter derivation in 1960. Kalman filtering applies to a wide range of problems including engineering, finance, and economics.

2. SCOPE AND APPLICABILITY

2.1 Motivation for Research

Multiple mathematical models developed for rotor blade fault and damage identification include neural networks, fuzzy logic systems, and Kalman filters. Recent research indicates that only the neural network approach has been applied to FRR algorithms, and that a Hidden Markov Model (HMM) approach outperformed the neural network. The utilization of mathematical modeling for FRR is similar to the damage identification method. Clearly defined criteria identify each flight regime considered, in the same way that clearly defined criteria identify different damage causes or locations. A recently developed code utilizes HMM to perform FRR. A regime prediction algorithm, based on Kalman filters, integrated the HMM FRR code to expand its HUMS application. This combined code uses the Kalman filters for prediction of the future flight parameters though, not for FRR algorithms.

Much of the FRR research performed throughout the past ten years is not available in the public domain. FRR algorithms and results remain classified by the government or proprietary to Original Equipment Manufacturers (OEM). The public domain FRR research typically focuses on post-processing algorithms rather than real-time regime recognition. The post processing codes also appear to use discrete algorithms, which do not clearly identify transitions between regimes. The HMM regime recognition code, although real-time, does have some difficulty identifying regime transitions that were not performed in its training data set.

2.2 Problem Statement

The problem examined by this research uses Kalman filtering to perform FRR, a technique not yet explored in public domain HUMS research. The primary purpose of this research is to develop a mathematical model for FRR, which uses Kalman Filtering to perform the regime recognition. The Kalman filter will identify the current flight regime and a graphical display will allow for the observation of real-time transitions between regimes. A secondary purpose is to advance the public domain knowledge of FRR algorithms. Major assumptions for

this study include limiting the flight spectrum to a commercial spectrum and limiting the rotorcraft of interest to a reciprocating single-engine helicopter.

This research aims to bridge the gap between the application of mathematical models for RCDT and HUMS, as well as advance public domain FRR algorithms. Rotor blade fault and damage identification applies multiple mathematical models. Yet only recently have FRR algorithms applied these models. The success of the HMM approach to FRR indicates that a similar approach which utilizes Kalman filtering should be successful. Additionally, much of the public domain FRR research focuses on post processing algorithms rather than real-time regime recognition. The post processing codes appear to use discrete algorithms, which do not clearly identify transitions between regimes.

2.3 Review of Related Literature

Multiple mathematical models developed for rotor blade fault and damage identification include neural networks, fuzzy logic systems, and Kalman filters. A review of available literature indicates that only the neural network approach has been applied to real-time FRR codes, and it was outperformed by a HMM. The neural network approach for damage identification combines a detailed physics-based model of rotor blades in forward flight with two neural networks. The neural networks in this study were trained first using ideal data and then trained using noisy data. Training the neural networks with noisy data allowed them to provide good damage estimates with noisy input data [4]. The feedforward neural networks used allow for modeling of complex relationships between the inputs and outputs and can model any given function. Drawbacks to neural networks include difficulty in understanding and developing the neural network, large amounts of time needed to train the neural network, and the training algorithms are difficult to understand and develop. Neural networks could be used for the mathematical modeling needed in this study, but the development difficulty and time required do not allow for practical application.

The researchers who developed the damage identification neural network approximated this system using a fuzzy logic system. Fuzzy logic systems can approximate any function and their research indicated that fuzzy logic systems could accurately estimate neural networks. The fuzzy logic system used the same physics-based model of the rotor in forward

flight. The fuzzy logic system accounts for noise and uncertainty in the data with acceptable accuracy. The fuzzy logic system was developed more quickly than the neural network using a defined set of fuzzy rules to determine each damage type. The fuzzy logic system identified the most likely fault using maximum matching defuzzification [5]. The fuzzy logic system could be used for regime identification needed for this study. However, lack of experience with fuzzy logic systems would increase the code development time required, thus a fuzzy logic system was not chosen for this study.

The Kalman filtering approach used for damage identification is a multiple-model adaptive estimation technique. This approach identifies four fault cases and an undamaged case. Faults were determined to be at one of four locations along the blade span with sensors simulated at eleven locations. The filters identified the fault type and most likely location. This technique used Kalman filters tuned to each fault type identified to obtain state estimates and residual vectors. The residual vectors were used to obtain a probability value for the most likely fault encountered. Theoretically, the lowest residual vector corresponds to the fault with the highest probability of occurrence [6]. Kalman filtering techniques inherently treat measurement and process noise, thus good parameter estimates from the data acquisition system are not required. Additionally, real-time systems regularly implement Kalman filters, thus a real-time FRR code can utilize Kalman filtering. Kalman filters are well understood by the thesis advisor, thus the filter development time will be less than with neural networks or fuzzy logic systems.

Current public domain FRR research offers little insight into code development. The research does include valuable information on regime and parameter sets. Each research organization has developed its own set of identified regimes. The regimes identified by the US Navy are general commercial spectrum regimes identified by their listed parameter set [7]. The report published by the US Navy does not appear to have any follow on data or studies and thus the parameter set and regime set outlined were not selected for this study.

Bell Helicopter Textron, Inc began FRR research as early as 1996. Three reports have been published based on this research using Bell model 412 rotorcraft in three distinct mission profiles [8][9][10]. All three reports outline the regime set identified and two of the reports outline the parameter set utilized. Additionally, one of the reports outlines a low airspeed regime recognition technique, which can capture both low speed flight maneuvers and hover

maneuvers [10]. The regime and parameter sets used in the most recent reports provided the basis for the regime and parameter set used in this study. Additionally, initial code development for this study used the decision tree method and limits identified by the July 2004 report [9]. These decisions correspond to the identification of the main flight regime using limits published in the report.

The results of the Bell Helicopter FRR research are included in a spectrum comparison for the three missions and the certification spectrum [10]. The results indicate that the different mission profiles have very different usage spectrums. The Atlanta Short Haul mission tended to be more damaging than the certification spectrum, while the Morgan City and Gulf Coast missions tended to be less damaging than the certification spectrum. The Bell studies utilized a Bell 412 rotorcraft, which is a twin-engine turbine rotorcraft, while this study will focus on a single-engine reciprocating rotorcraft.

Two FRR papers released during the course of this thesis deserve mentioning. The first paper details a FRR algorithm, which uses HMM to perform the regime recognition [11]. The HMM approach to FRR uses a HMM tuned to each flight regime. The model training data was from an Army UH-60L helicopter and was military spectrum. The study used additional data from the UH-60L to test the HMM. This test data was used to compare the HMM with other mathematical approaches including neural networks, discriminant analysis, regression trees, naïve bayes, and k-nearest neighbor. The HMM method significantly outperformed all other methods. The HMM is developed similarly to the Kalman filter with the training and testing stages.

The second paper uses Kalman filtering to predict the future flight parameters and feeds this parameter estimation to the HMM described in the first paper [12]. The regime prediction approach is not a new FRR algorithm; rather it is an extension of regime recognition. A Kalman filter estimates the rate of change of the flight parameters. The parameter value for the next time step is estimated using this rate of change. The estimated parameters are then input to the HMM for regime recognition, and the predicted regimes are output. The regime prediction approach maintains 93% accuracy with ten seconds of future prediction; however, this accuracy drops steadily after ten seconds. The advantage of regime prediction is the ability to warn a pilot of a damaging maneuver before entering the maneuver. One highlighted application of the

regime prediction is for heavy lift maneuvers. The regime prediction algorithm could alert the pilot if the power required is greater than the power generated.

Although the two papers mentioned above perform analysis on a military flight spectrum, it is conceivable that a commercial spectrum could be modeled using these methods. Additionally the Kalman filtering approach to FRR developed in this thesis could apply the regime prediction method described in the second paper. The training helicopters used to gather the commercial flight spectrum data for this thesis could utilize the regime prediction to alert student pilots to potentially damaging flight conditions. Thus, the FRR algorithm developed herein will represent an important advancement in public domain FRR research.

2.4 Hypothesis

FRR algorithms must be developed to identify commercial spectrum rotorcraft maneuvers using recorded flight parameters. The FRR code will utilize real-time Kalman Filters to determine the regime flown. Post processing analysis will verify the real-time processing performed by the FRR algorithms and Kalman Filters. Additionally a graphical interface will be developed to show the identified regime in real-time.

If the FRR algorithms perform properly then the correct regime will be identified and verified both in real-time and post processing. If the FRR algorithms and graphical interface perform properly then real-time transitions between regimes will be observed on the graphical interface. If the FRR algorithms and Kalman filters perform properly then the application of Kalman filters to FRR algorithms will be successful and represent an advancement of FRR technologies.

3. METHODS

3.1 Design and Instrumentation

The intended regime set for this study is adapted from the studies performed by Bell Helicopter Textron, Inc [9] and is included in Appendix B. The intended flight parameter set for this study is adapted from the Schweizer 300 Flight Test program performed by the Embry-Riddle Aeronautical University (ERAU) HUMS team is included in Appendix C. All code development will be performed using Mathworks MATLAB and Simulink. Representative data will be obtained using the Schweizer 300 Flight Test Data gathered by the ERAU HUMS team. Real-time processing of the data will be performed using a COTS PC.

3.2 Data Analysis

The COTS PC will utilize a Matlab code that reads in the HUMS data using look up tables. The data will be played through the Kalman filter. The filter will identify the performance index for each regime identified. These performance index values are displayed to the user via graphical interface and vary in real-time. The state estimates of the Kalman filter will be graphed during the flight using Matlab and the graph can be observed once the flight is completed. The state estimates of the Kalman filter will be saved to an Excel file for post processing.

4. PROCEDURE

The development of a Kalman filter for FRR begins with determining the type of system modeled. In this case, the Kalman filter will output a performance index for each identified regime. This performance index is a constant, which changes during the flight based on the flight parameters. A zero order polynomial models the estimation of a constant using differential equations.

4.1 General Differential Equations for Zero Order Polynomial

The estimation of a flight regime from measured flight parameters uses differential equations to estimate a zero-order polynomial. In this case the flight regime estimate is a constant value, $x = a_0$. The constant is a performance index, which represents the potential that the rotorcraft is in that regime. In general for a polynomial $\dot{x} = Fx + w$, where \dot{x} is the derivative of x , F is the system dynamics matrix which relates the derivative to the value of x , and w is a white Gaussian noise distribution. For a zero order polynomial $\dot{x} = 0$, but $x \neq 0, w \neq 0$, thus $F = 0$.

4.2 General Equations for a Discrete Kalman Filter

The Kalman filter used for this study is a discrete filter. Thus instead of estimating \dot{x} , it estimates x_k , which represents the value of x at the next time step. The general filter equations for a Discrete Kalman Filter are:

$$\begin{aligned}z_k &= Hx_k + v_k \\ \hat{x}_k &= \Phi_k \hat{x}_{k-1} + w_k \\ \hat{x}_k &= \Phi_k \hat{x}_{k-1} + K_k (z_k - H\Phi_k \hat{x}_{k-1})\end{aligned}$$

Additionally the Riccati Equations for a Discrete Kalman Filter are:

$$M_k = \Phi_k P_{k-1} \Phi_k^T + Q_k$$

$$K_k = M_k H^T (H M_k H^T + R_k)^{-1}$$

$$P_k = (I - K_k H) M_k$$

Any Kalman filtering text that discusses filter development and application should contain these equations [13]. This thesis does not derive the discrete Kalman filter equations, rather it presents an application of the equations. The Kalman filter developed for this thesis calculates the last four equations listed above. The first two equations were used during the filter tuning process.

4.3 General Discrete Kalman Filter for FRR

The Kalman filter developed for this study outputs an estimated performance index value for each flight regime, \hat{x}_k , where the number of flight regimes is $\hat{x}_k = \{\hat{x}_{k_1}; \hat{x}_{k_2}; \dots; \hat{x}_{k_n}; \dots; \hat{x}_{k_m}\}$. The estimated performance index corresponds to the state estimate in Kalman filtering theory. The estimated performance index value for a particular flight regime will increase as the filter determines that this is the regime currently being flown, and decrease at the rotorcraft leaves that flight regime. One specific criterion for the FRR Kalman filter developed herein is that it must calculate these performance indices independently of one another.

The filter measurement inputs for this study are the rotorcraft flight parameters, z_k . The number of flight parameters $z_k = \{z_{k_1}; z_{k_2}; \dots; z_{k_n}; \dots; z_{k_m}\}$, are those parameters which can be used to identify a particular flight regime. The number of flight parameter inputs must be the same as the number of regimes identified to ensure that the matrices used within the filter remain square. It is possible for one parameter to help determine multiple regimes, however this makes the performance indices of the regimes dependent upon one another.

The filter signal variance inputs for this study are the sensor manufacturer's sensitivity values, r_k . The signal variance matrix is an $n \times n$ diagonal matrix of the r_k values. The filter interprets the signal variance values as a weighting factor for each measurement. Smaller signal

variance values indicate a more accurate measurement, and thus that measurement more heavily determines the performance index estimates.

$$r_k = \begin{bmatrix} r_k & 0 & 0 & 0 & 0 & 0 & 0 & 0 \\ 0 & r_k & 0 & 0 & 0 & 0 & 0 & 0 \\ 0 & 0 & 0 & 0 & 0 & 0 & 0 & 0 \\ 0 & 0 & 0 & 0 & 0 & 0 & 0 & 0 \\ 0 & 0 & 0 & 0 & r_k & 0 & 0 & 0 \\ 0 & 0 & 0 & 0 & 0 & 0 & 0 & 0 \\ 0 & 0 & 0 & 0 & 0 & 0 & 0 & 0 \\ 0 & 0 & 0 & 0 & 0 & 0 & 0 & r_k \end{bmatrix}$$

The filter input values for initial covariance, $P_{k_{est}}$, are large to allow the filter to converge on a solution after some time. The filter interprets large initial covariance values as a large uncertainty in the initial performance index estimates. Due to this uncertainty, the filter will utilize the measurements to obtain more accurate performance index estimates. The initial performance index estimates, $\hat{x}_{k_{est}}$, are zero which is interpreted by the filter as uncertainty in these initial estimates.

$$P_{k_{est}} = \begin{bmatrix} P_{k_{est}} & 0 & 0 & 0 & 0 & 0 & 0 & 0 \\ 0 & P_{k_{est}} & 0 & 0 & 0 & 0 & 0 & 0 \\ 0 & 0 & 0 & 0 & 0 & 0 & 0 & 0 \\ 0 & 0 & 0 & 0 & 0 & 0 & 0 & 0 \\ 0 & 0 & 0 & 0 & P_{k_{est}} & 0 & 0 & 0 \\ 0 & 0 & 0 & 0 & 0 & 0 & 0 & 0 \\ 0 & 0 & 0 & 0 & 0 & 0 & 0 & 0 \\ 0 & 0 & 0 & 0 & 0 & 0 & 0 & P_{k_{est}} \end{bmatrix}$$

$$\hat{x}_{k_{est}} = \begin{bmatrix} \hat{x}_{k_{est}} \\ \hat{x}_{k_{est}} \\ 0 \\ 0 \\ \hat{x}_{k_{est}} \\ 0 \\ 0 \\ \hat{x}_{k_{est}} \end{bmatrix}$$

The filter process noise inputs, Q_k , for this study are assumed to be white Gaussian noise with a zero-mean distribution. The process noise is represented by an $n \times n$ diagonal matrix of the Q_k values. The filter interprets the process noise values as uncertainty in the performance index estimate based on the equations used to model the system. This uncertainty allows the filter to account for short-duration parameter jumps without causing the performance index estimate to jump. For example, if a large pitch rate occurs for a short amount of time, from a wind gust, during level flight the filter would continue to estimate level flight rather than a short duration climb.

$$Q_k = \begin{bmatrix} Q_k & 0 & 0 & 0 & 0 & 0 & 0 \\ 0 & Q_k & 0 & 0 & 0 & 0 & 0 \\ 0 & 0 & 0 & 0 & 0 & 0 & 0 \\ 0 & 0 & 0 & 0 & 0 & 0 & 0 \\ 0 & 0 & 0 & 0 & Q_k & 0 & 0 \\ 0 & 0 & 0 & 0 & 0 & 0 & 0 \\ 0 & 0 & 0 & 0 & 0 & 0 & 0 \\ 0 & 0 & 0 & 0 & 0 & 0 & Q_k \end{bmatrix}$$

The state transition matrix, Φ_k , is the connection between the performance index estimate at the current time step and the performance index estimate at the next time step. The FRR Kalman filter has no a priori information about the future flight regimes, nor does it have a posteriori information about the past flight regimes. The best estimate for the performance index at the next time step is that it will be the same as the current time step, thus the state transition matrix is an identity matrix.

$$\Phi_k = \begin{bmatrix} \Phi_k & 0 & 0 & 0 & 0 & 0 & 0 \\ 0 & \Phi_k & 0 & 0 & 0 & 0 & 0 \\ 0 & 0 & 0 & 0 & 0 & 0 & 0 \\ 0 & 0 & 0 & 0 & 0 & 0 & 0 \\ 0 & 0 & 0 & 0 & \Phi_k & 0 & 0 \\ 0 & 0 & 0 & 0 & 0 & 0 & 0 \\ 0 & 0 & 0 & 0 & 0 & 0 & 0 \\ 0 & 0 & 0 & 0 & 0 & 0 & \Phi_k \end{bmatrix}$$

The connection matrix, H_k , is the connection between the measured flight parameters and the performance index estimate. The connection matrix is determined based on how the flight parameter will affect the decision for the performance index. For example, if a parameter clearly indicates a particular regime, and only that regime, then the row of the connection matrix for that parameter and column for that regime would be approximately one. All other columns for that parameter and rows for that regime would be zero. If the connection matrix is a diagonal matrix, each parameter determines only one regime and thus the performance indices are entirely independent of one another.

$$H_k = \begin{bmatrix} H_{k_1} & 0 & 0 & 0 & 0 & 0 & 0 & 0 \\ 0 & H_{k_2} & 0 & 0 & 0 & 0 & 0 & 0 \\ 0 & 0 & 0 & 0 & 0 & 0 & 0 & 0 \\ 0 & 0 & 0 & 0 & 0 & 0 & 0 & 0 \\ 0 & 0 & 0 & 0 & H_{k_3} & 0 & 0 & 0 \\ 0 & 0 & 0 & 0 & 0 & 0 & 0 & 0 \\ 0 & 0 & 0 & 0 & 0 & 0 & 0 & 0 \\ 0 & 0 & 0 & 0 & 0 & 0 & 0 & H_{k_4} \end{bmatrix}$$

The general discrete FRR Kalman filter inputs and outputs listed above were used to develop the Schweizer 300 FRR Kalman filter. It is important that the performance indices be calculated independently of one another to demonstrate the effectiveness of the FRR Kalman filter. The FRR algorithms discussed in the Section 2.3 Review of Related Literature use independent regimes. The calculation of independent regimes is rather simple for a discrete FRR algorithm but contributes to the lack of regime transition identification. The FRR algorithm developed herein uses a discrete Kalman filter for a continuous recognition application. The FRR Kalman filter should be able to calculate regimes independently while allowing the user to observe real-time regime transitions.

4.4 Flow Chart of Discrete FRR Kalman Filter Equations

The following flow chart, Figure 1, depicts the course of data through the FRR Kalman filter. The flow chart highlights major equations calculated, filter inputs, and filter outputs. The

FRR Kalman filter runs at 10Hz. This calculation rate is sufficient because the Schweizer 300 sample rate was 6Hz for all data captured by the HUMS.

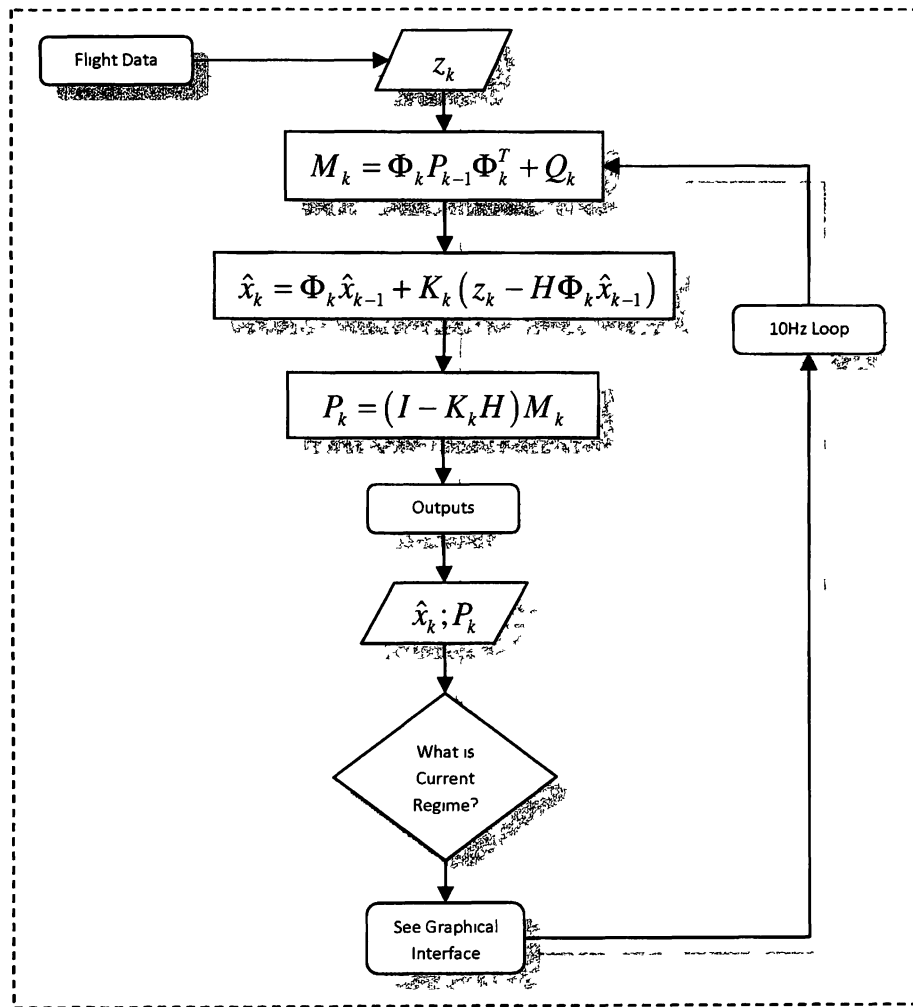


Figure 1: Flowchart of Equations for FRR Kalman Filter

The following screenshots represent the FRR Kalman filter Simulink model. Figure 2 is the model top level. This figure shows the flight parameters and the scaling used on these inputs. Figure 3 shows the top level of the Kalman filter. The four Kalman filtering equations are calculated within this portion of the model.

4.5 Sample Kalman Filter for FRR

The following example is the filter used to analyze the Schweizer 300 flight test data. Sample input and output data vectors are provided with this example, however, Section 5.2 Post Processing Regime Specific FRR discusses the regime identification in further detail.

4.5.1 Inputs

The following aircraft parameters, selected from the flight data recorded on the Schweizer 300, each identify a single regime. The model scales the input parameters such that they are all on the same order of magnitude.

$$z_k = \begin{bmatrix} W_{positive} \\ WOW \\ IAS^{-1} \\ IAS \\ ROC_{negative} \\ \phi_{negative} \\ \phi_{positive} \\ ROC_{0 \rightarrow 100 \text{ fpm}}^{-1} \end{bmatrix}$$

The following signal variance matrix uses values obtained from the published sensor specifications and outlined in the Installation Document for the Schweizer 300 flight test [14].

$$r_k = \begin{bmatrix} 0.066 \frac{ft}{s} & 0 & 0 & 0 & 0 & 0 & 0 & 0 \\ 0 & 1 \times 10^{10} & 0 & 0 & 0 & 0 & 0 & 0 \\ 0 & 0 & 1kr & 0 & 0 & 0 & 0 & 0 \\ 0 & 0 & 0 & 1kr & 0 & 0 & 0 & 0 \\ 0 & 0 & 0 & 0 & 3.94 \frac{ft}{min} & 0 & 0 & 0 \\ 0 & 0 & 0 & 0 & 0 & 0.015^\circ & 0 & 0 \\ 0 & 0 & 0 & 0 & 0 & 0 & 0.015^\circ & 0 \\ 0 & 0 & 0 & 0 & 0 & 0 & 0 & 3.94 \frac{ft}{min} \end{bmatrix}$$

The following process noise values, determined by experience with the Kalman filter, ensure that the filter can handle short duration parameter jumps.

$$Q_t = \begin{bmatrix} 0.001 & 0 & 0 & 0 & 0 & 0 & 0 & 0 \\ 0 & 0.001 & 0 & 0 & 0 & 0 & 0 & 0 \\ 0 & 0 & 0.001 & 0 & 0 & 0 & 0 & 0 \\ 0 & 0 & 0 & 0.001 & 0 & 0 & 0 & 0 \\ 0 & 0 & 0 & 0 & 0.001 & 0 & 0 & 0 \\ 0 & 0 & 0 & 0 & 0 & 0.001 & 0 & 0 \\ 0 & 0 & 0 & 0 & 0 & 0 & 0.001 & 0 \\ 0 & 0 & 0 & 0 & 0 & 0 & 0 & 0.001 \end{bmatrix}$$

The following state transition matrix estimates that the next flight regime will be the same as the current flight regime based on the lack of a priori information.

$$\Phi_t = \begin{bmatrix} 1 & 0 & 0 & 0 & 0 & 0 & 0 & 0 \\ 0 & 1 & 0 & 0 & 0 & 0 & 0 & 0 \\ 0 & 0 & 1 & 0 & 0 & 0 & 0 & 0 \\ 0 & 0 & 0 & 1 & 0 & 0 & 0 & 0 \\ 0 & 0 & 0 & 0 & 1 & 0 & 0 & 0 \\ 0 & 0 & 0 & 0 & 0 & 1 & 0 & 0 \\ 0 & 0 & 0 & 0 & 0 & 0 & 1 & 0 \\ 0 & 0 & 0 & 0 & 0 & 0 & 0 & 1 \end{bmatrix}$$

The following initial covariance values allow the filter to converge on the performance index estimates. Large values in the covariance matrix indicate that the filter is unsure about the initial state estimates and should weight the current parameter measurements more heavily than the state estimate to determine the next state estimate.

$$P_{t_0} = \begin{bmatrix} 99999 & 0 & 0 & 0 & 0 & 0 & 0 & 0 \\ 0 & 99999 & 0 & 0 & 0 & 0 & 0 & 0 \\ 0 & 0 & 99999 & 0 & 0 & 0 & 0 & 0 \\ 0 & 0 & 0 & 99999 & 0 & 0 & 0 & 0 \\ 0 & 0 & 0 & 0 & 99999 & 0 & 0 & 0 \\ 0 & 0 & 0 & 0 & 0 & 99999 & 0 & 0 \\ 0 & 0 & 0 & 0 & 0 & 0 & 99999 & 0 \\ 0 & 0 & 0 & 0 & 0 & 0 & 0 & 99999 \end{bmatrix}$$

The following initial state values were chosen because there is no certainty about what flight regime will be the current regime when the filter begins receiving data. These values allow the filter to converge on a more appropriate state estimate.

$$\hat{x}_{k_{est}} = \begin{bmatrix} 0 \\ 0 \\ 0 \\ 0 \\ 0 \\ 0 \\ 0 \\ 0 \\ 0 \end{bmatrix}$$

The following connection matrix determines the flight regime performance index estimates independently of one another. Additionally, the input flight parameters solely calculate the flight regime performance indices. To ensure that the performance index value would be large when the flight parameter value was large the connection matrix values are nearly 1. This indicates that the performance index value will be nearly 100% of the flight parameter value. This matrix is tuned to the flight data specific to the Schweizer 300.

$$H_k = \begin{bmatrix} 00 & 00 & 09 & 00 & 00 & 00 & 00 & 00 & 00 \\ 09 & 00 & 00 & 00 & 00 & 00 & 00 & 00 & 00 \\ 00 & 00 & 00 & 00 & 00 & 00 & 00 & 00 & 09 \\ 00 & 00 & 00 & 00 & 00 & 00 & 08 & 00 & 00 \\ 00 & 00 & 00 & -09 & 00 & 00 & 00 & 00 & 00 \\ 00 & 00 & 00 & 00 & 00 & -08 & 00 & 00 & 00 \\ 00 & 00 & 00 & 00 & 08 & 00 & 00 & 00 & 00 \\ 00 & 09 & 00 & 00 & 00 & 00 & 00 & 00 & 00 \end{bmatrix}$$

The number of flight regimes identified provides the dimensions for the identity matrix used by the filter.

$$I = \begin{bmatrix} 1 & 0 & 0 & 0 & 0 & 0 & 0 & 0 \\ 0 & 1 & 0 & 0 & 0 & 0 & 0 & 0 \\ 0 & 0 & 1 & 0 & 0 & 0 & 0 & 0 \\ 0 & 0 & 0 & 1 & 0 & 0 & 0 & 0 \\ 0 & 0 & 0 & 0 & 1 & 0 & 0 & 0 \\ 0 & 0 & 0 & 0 & 0 & 1 & 0 & 0 \\ 0 & 0 & 0 & 0 & 0 & 0 & 1 & 0 \\ 0 & 0 & 0 & 0 & 0 & 0 & 0 & 1 \end{bmatrix}$$

4.5.2 Outputs

The Kalman filter can identify the regimes listed below. It is important to note that a maneuver combining the regimes below, such as a high speed descending left turn, will have high performance index values for all of the identified regimes.

$$\hat{x}_k = \begin{bmatrix} OnGround \\ Level \\ Climb \\ Descend \\ RightTurn \\ LeftTurn \\ HighSpeed \\ LowSpeed \end{bmatrix}$$

4.5.3 Sample Data

The following vectors represent sample input and output data for the FRR Kalman Filter. The scaled aircraft parameters are the input data and the performance indices are the output data. The regime identified is High Speed flight. Figure 4 is a graph of the performance indices and confirms that the rotorcraft FRR algorithm has identified High Speed flight for the time snapshot indicated. The input and output vectors are from time step 603.

$$z_k = \begin{bmatrix} 0 \\ 0 \\ 0.331963 \\ 42.17341 \\ -4.00525 \\ -2.5747 \\ 0 \\ 2.496723 \end{bmatrix} \quad \hat{x}_k = \begin{bmatrix} 0 \\ 5.762137 \\ 0.049995 \\ 1.583834 \\ 0 \\ 2.806889 \\ 51.45755 \\ 0.377887 \end{bmatrix}$$

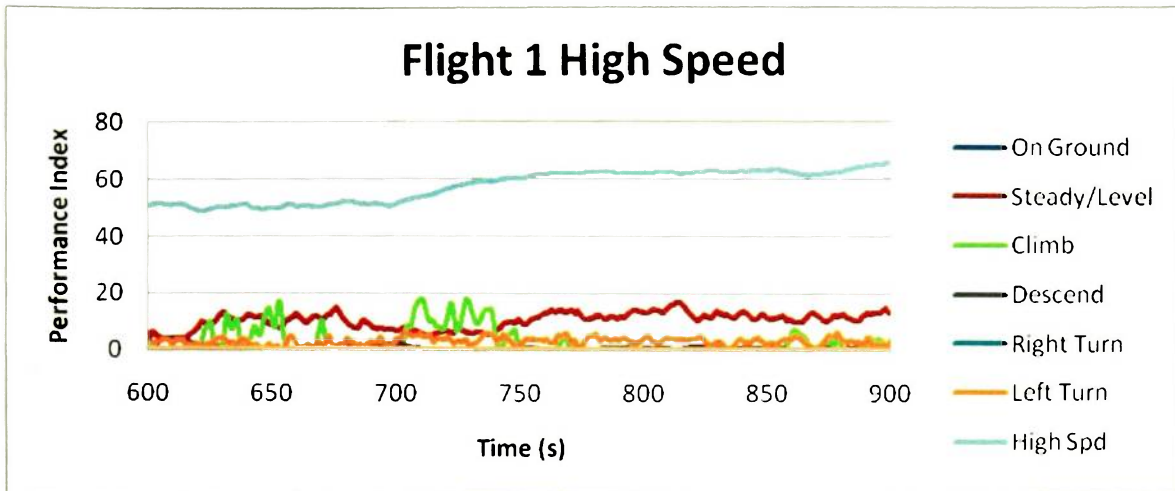


Figure 4: Sample FRR Identification

The sample identification shown in Figure 4 clearly indicates High Speed as the most likely regime. There appears to be some climbing during two instances 615 to 650 seconds and 700 to 750 seconds. The remaining time intervals indicate that the rotorcraft is also in Level flight. The event code within the flight test data confirmed that the rotorcraft was in High Speed Level flight during this time interval.

5. ANALYSIS

The FRR algorithm developed for this study enables the user to perform real-time or post processing analysis. The real-time FRR analysis performed for this study allows the user to observe the identified regime and transitions between regimes via the real-time display. Post processing regime specific analysis of the FRR data highlights the dominant regime determination and identifies combination maneuvers. Post processing regime transition identification focuses on the observation of regime transitions during snapshot time intervals. The final analysis technique presented demonstrates the affect of varying the process noise input on the regime identification and observation of regime transitions. The post processing analysis utilize the Excel data files created upon completion of a Schweizer 300 flight by the FRR algorithm.

5.1 Real-Time FRR via Display

The FRR real-time analysis focuses on the observation of the identified regimes and transitions between the regimes. The real-time graphical display needs to be user-friendly and have at-a-glance readability. The following figures are snapshots of the real-time display. The highest bar represents the current identified regime. The bar heights change as the performance indices change, thus the transition between regimes is observable.

5.1.1 Single Regime Identification

Figure 5 represents the real-time identification that the rotorcraft is on the ground. The figure shows that On Ground is the highest performance index. The other performance indices indicated are High Speed and Low Speed. Although the speed based performance indices are non-zero, they are significantly lower than On Ground. In this situation, the user deduces that the rotorcraft is, in fact, on the ground. The on ground condition is readily verifiable in real-time by a pilot or test engineer.

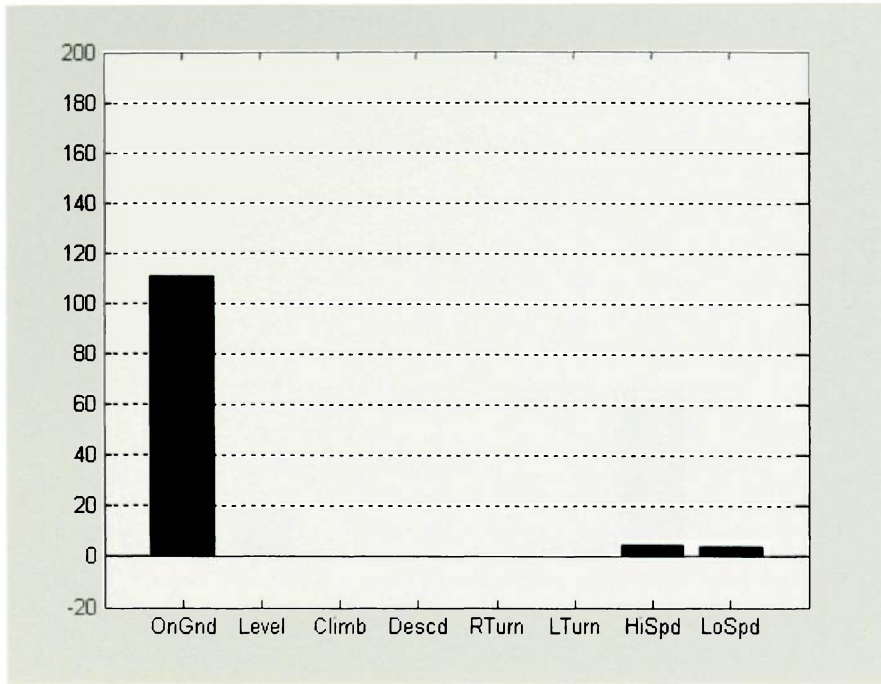


Figure 5: Real-Time On Ground Recognition

Figure 6 represents the real-time identification that the rotorcraft is in high-speed flight. The figure shows that High Speed is the highest performance index. The other performance indices indicated are Level Flight and Left Turn. Although these performance indices are non-zero, they are significantly lower than High Speed. Additionally, the Level Flight performance index is higher than the Left Turn performance index. In this situation, the user deduces that the rotorcraft is, in fact, in high-speed flight. The user can also reason that the rotorcraft is in Level Flight. Thus, the real-time FRR is that the rotorcraft is in High Speed Level Flight. The high-speed level flight condition is readily verifiable in real-time by a pilot or test engineer.

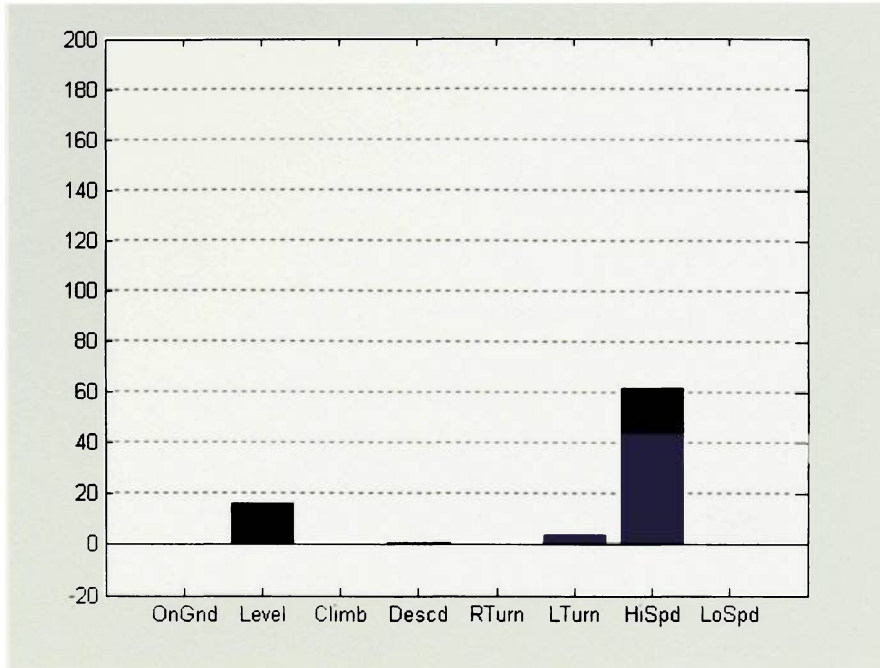


Figure 6: Real-Time High Speed Level Recognition

Figure 7 represents the real-time identification that the rotorcraft is in low-speed level flight. The figure shows that Low Speed and Level Flight are the highest performance indices. The other performance indices indicated are Left Turn and High Speed. Although these performance indices are non-zero, they are significantly lower than Low Speed and Level Flight. The Level Flight and Low Speed performance indices are nearly the same value. In this situation, the user deduces that the rotorcraft is in low-speed level flight. Neither Low Speed nor Level Flight is the dominant regime, however, they are both dominant over the remaining regimes. Thus, the real-time FRR is that the rotorcraft is in Low Speed Level Flight. The low-speed level flight condition is readily verifiable in real-time by a pilot or test engineer.

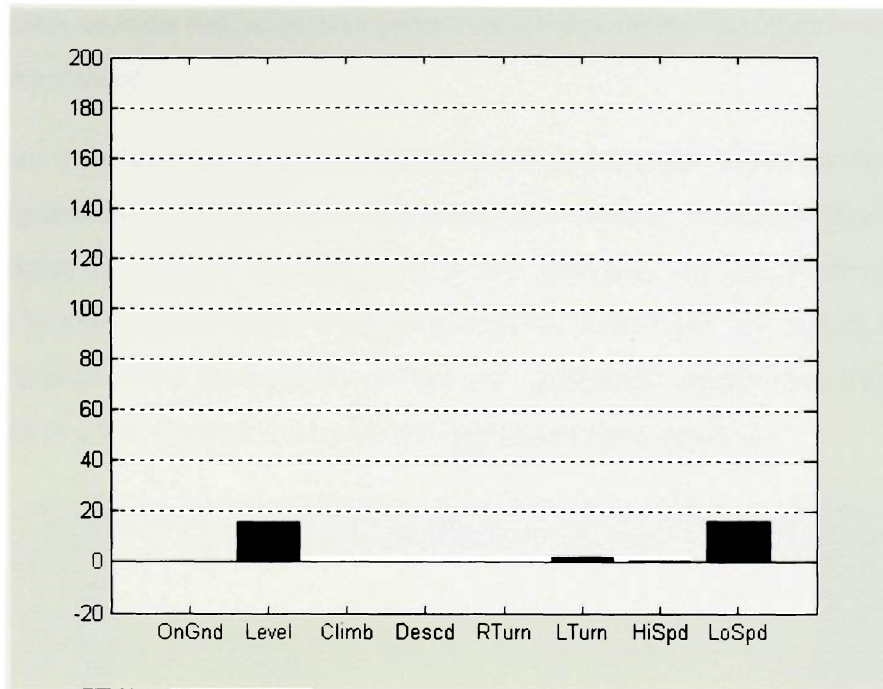


Figure 7: Real-Time Low Speed Level Recognition

Figure 7 represents the real-time condition that the performance index values for the dominant regimes are not significantly large values, but are the largest of the indicated values. In this situation, the user estimates that the largest performance indices still indicate the current regime. Additionally, Figure 6 and Figure 7 demonstrate that the rotorcraft is rarely in a single regime. The real-time display shows the current value for performance index, and more than one index may have a large value. If more than one index is indicated, the user determines that a combination maneuver is being flown.

5.1.2 Combination Maneuver Identification

It is possible for the rotorcraft to perform a maneuver that combines several of the identifiable regimes. In this situation, the filter will first identify that the rotorcraft is or is not on the ground. Then, based on the input parameter values, it will identify the speed condition, low or high. The filter next identifies if the rotorcraft is turning, and if so, whether it is a right or left turn. Next, the algorithm determines if the rotorcraft is climbing or descending. Lastly, it recognizes if there is a level flight condition. The combination maneuver causes several performance indices to have high values, recognized in the order listed above. The graphical

display indicates multiple bars with close performance index values. The figures below represent compound maneuvers.

Figure 8 shows a high-speed climb. The performance index values for High Speed and Climb are significantly larger than the other performance indices. Additional regimes identified are Level Flight, Low Speed, and Left Turn. In this situation, the user determines that the rotorcraft is in a High Speed Climb. The user ignores the Level Flight, Low Speed, and Left Turn indications because their performance indices are significantly smaller than High Speed and Climb. The pilot or test engineer can verify the high-speed climb condition.

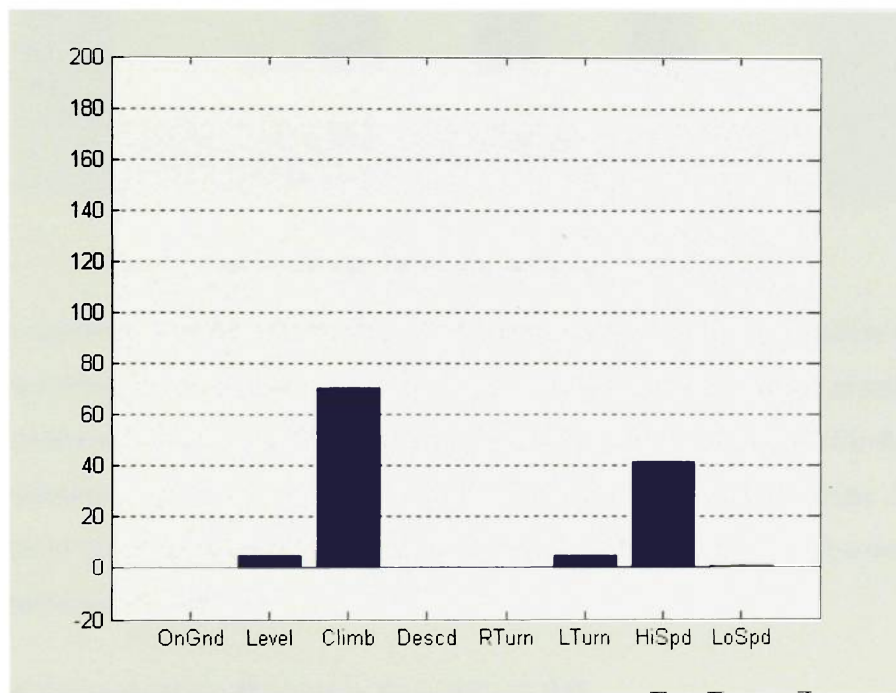


Figure 8: Real-Time High Speed Climb Recognition

Figure 9 shows a high-speed climbing right turn. The performance index values for High Speed, Climb, and Right Turn are significantly larger than the other performance indices. The additional regime identified is Level Flight. In this situation, the user determines that the rotorcraft is in a High Speed Climbing Right Turn. The user ignores the Level Flight indication because its performance index is significantly smaller than High Speed, Climb, and Right Turn. The pilot or test engineer can verify the high-speed climbing right turn condition.

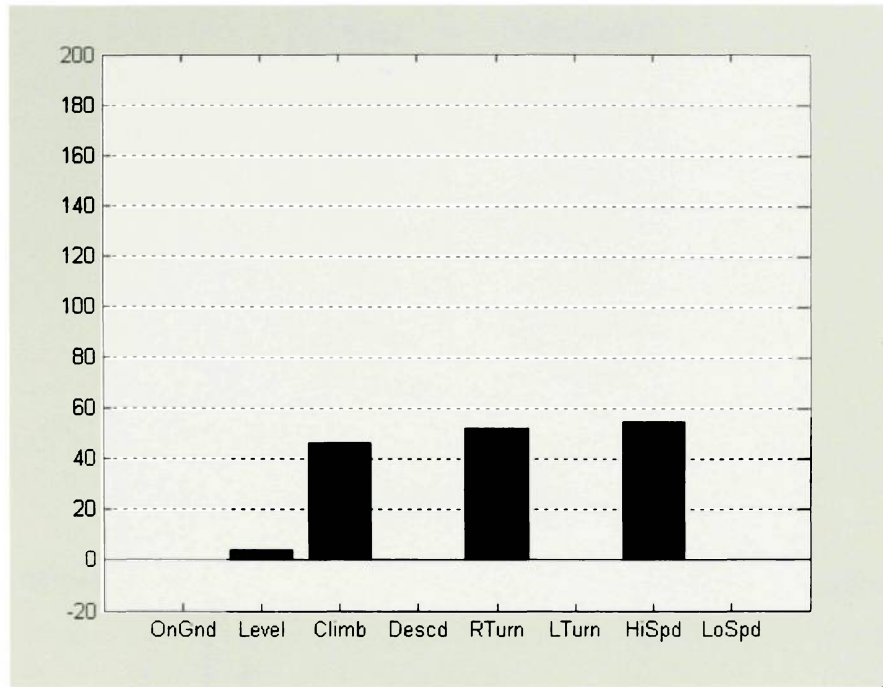


Figure 9: Real-Time High Speed Climbing Right Turn Recognition

The real-time analysis results described herein show that the application of a Kalman filter for a real-time FRR algorithm has been successful. Observation of regime identification and regime transitions has been the primary purpose of the real-time analysis. The figures above infer that real-time regime transitions are observable because the screenshots each show a different FRR. In order for different regimes to be identified the real-time display must show the transitions between the regimes.

5.2 Post Processing Regime Specific FRR

The following vectors represent input and output data for specific regimes. The inputs are the scaled flight parameters and the outputs are the performance indices for all regimes. The target regime should represent the highest performance index value for proper FRR by the Kalman filter. The vectors are presented in the following format. A snapshot graph for each regime identification is generated from the performance index Excel file.

$$z_k = \begin{bmatrix} w_{positive} \\ WOW \\ IAS^{-1} \\ IAS \\ ROC_{negative} \\ \phi_{negative} \\ \phi_{positive} \\ ROC_{0 \rightarrow 100 \text{ fpm}}^{-1} \end{bmatrix} \quad \hat{x}_k = \begin{bmatrix} OnGround \\ Level \\ Climb \\ Descend \\ RightTurn \\ LeftTurn \\ HighSpeed \\ LowSpeed \end{bmatrix}$$

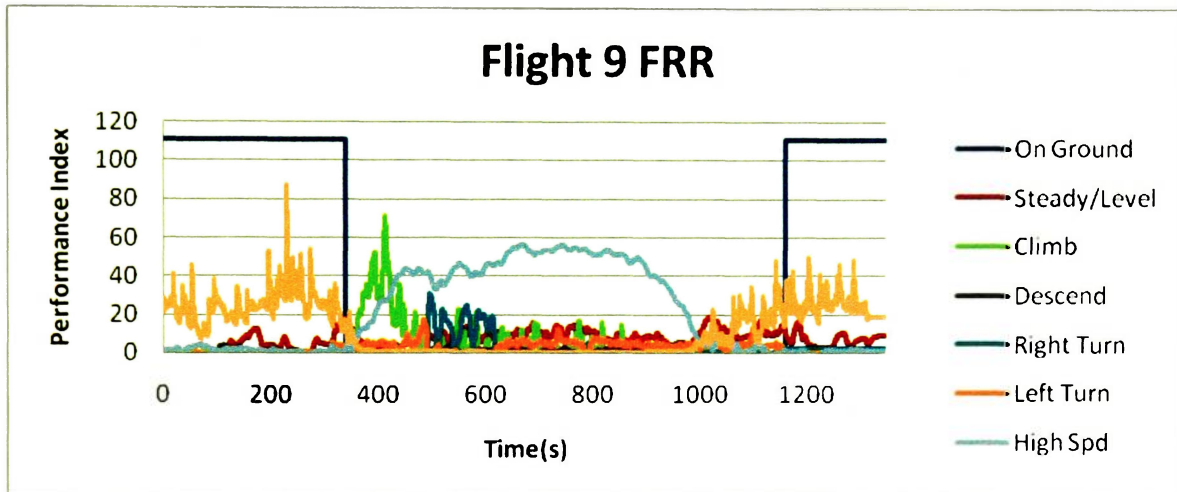


Figure 10: Sample FRR Graph

Figure 10 is the FRR for all of Flight 9. The graphs included with the individual regime identification are snapshots of time intervals. The snapshot graphs highlight the regime described and typically include some identification for additional regimes. The purpose of the snapshot graphs is to demonstrate proper identification of a single regime.

5.2.1 On Ground

A large value for WOW identifies that the rotorcraft is on the ground. While On Ground is the dominant regime, the user primarily ignores other regimes identified. The data below represents a typical On Ground identification. Figure 11 is a graph of the first 300 seconds of Flight 1. This selection contains On Ground and Steady Hover data, the input parameter and output regime values are from time step 118.1.

$$z_t = \begin{bmatrix} 0.528215 \\ 100 \\ 16.84276 \\ 0.831218 \\ 0 \\ -0.0929 \\ 0 \\ 17.02793 \end{bmatrix} \quad \hat{x}_t = \begin{bmatrix} 111.111 \\ 6.4297072 \\ 0.3953948 \\ 0.38493 \\ 0 \\ 0.1153 \\ 2.070015 \\ 22.90207 \end{bmatrix}$$

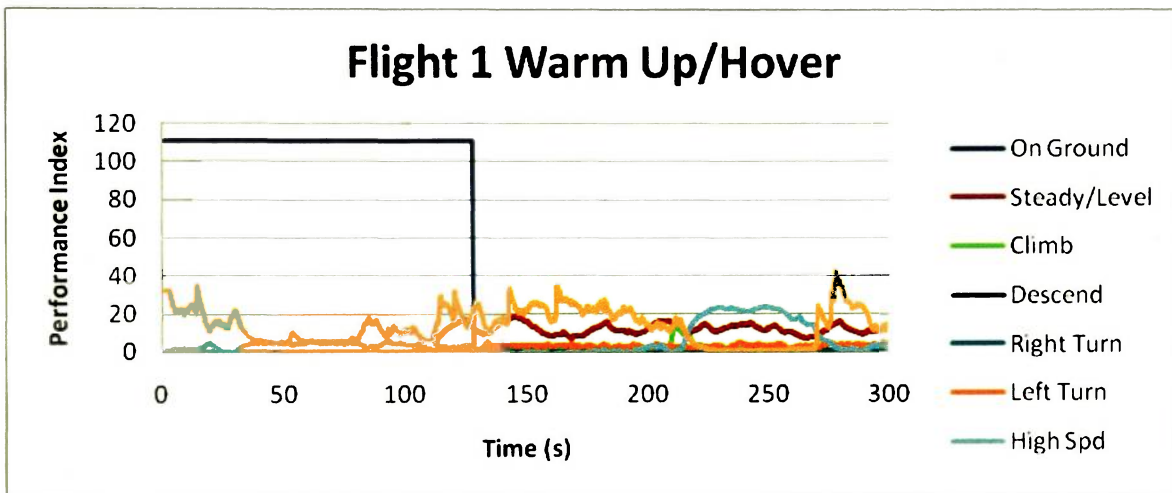


Figure 11: On Ground Identification

The WOW value is discrete represented by 0 and 100. The data above demonstrates that when the rotorcraft is on the ground prior to takeoff, WOW is the highest parameter value. The value for WOW is significantly larger than the other aircraft parameters, thus the performance index for On Ground is larger than the other performance indices. The next highest regimes, Low Speed and Level, correspond to the next highest parameter values.

Running Landing, shown in Figure 12, was one On Ground combination maneuver tested. During the running landing, the Low Speed performance index is also quite high. The data below represents the on ground identification of the running landing. Note the high value for the Low Speed Performance index compared to the typical On Ground identification above. The input parameter and output regime values are from time step 2176.2.

$$z_k = \begin{bmatrix} 0.479003 \\ 100 \\ 3.158484 \\ 4.432506 \\ 0 \\ -0.04972 \\ 0 \\ 4.008944 \end{bmatrix} \quad \hat{x}_k = \begin{bmatrix} 111.111 \\ 10.04921 \\ 1.246262 \\ 1.006049 \\ 0.002106 \\ 0.043321 \\ 14.9033 \\ 1.54123 \end{bmatrix}$$

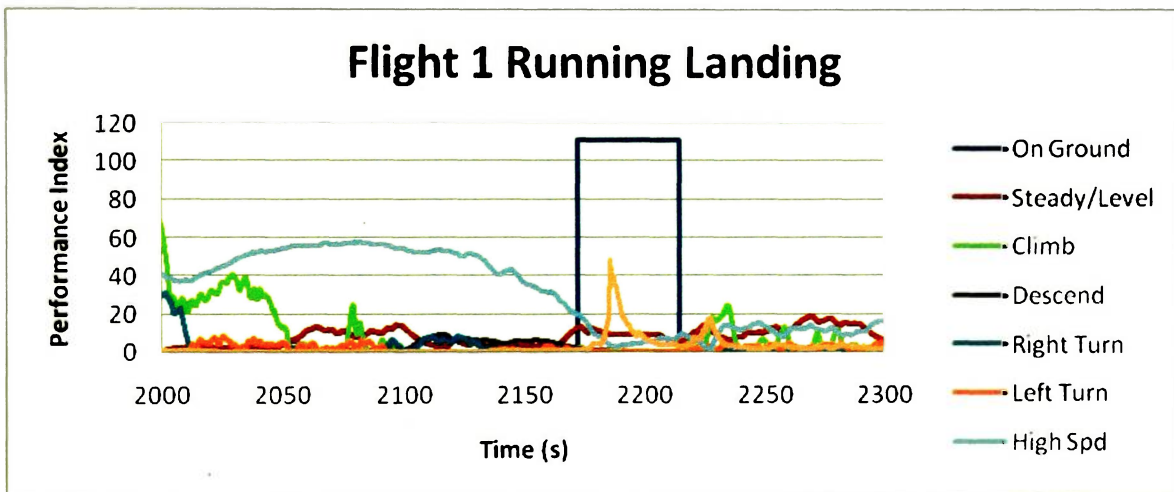


Figure 12: Running Landing Identification

Autorotation, shown in Figure 13, was the other On Ground combination maneuver tested. During a full-down autorotation, straight-in or turning, the Low Speed, High Speed, or Descend performance indices may also be rather large. The data below represents the end of a full-down autorotation. The FRR algorithm identifies the landing portion of the autorotation as On Ground, but the Low Speed performance index value is also large.

$$z_k = \begin{bmatrix} 0 \\ 100 \\ 19.59236 \\ 0.714564 \\ -0.03125 \\ 0 \\ 0.559 \\ 3.560748 \end{bmatrix} \quad \hat{x}_k = \begin{bmatrix} 111.111 \\ 4.578121 \\ 0.000549 \\ 0.466854 \\ 0.687933 \\ 4.33 \times 10^{-15} \\ 2.207211 \\ 35.45113 \end{bmatrix}$$

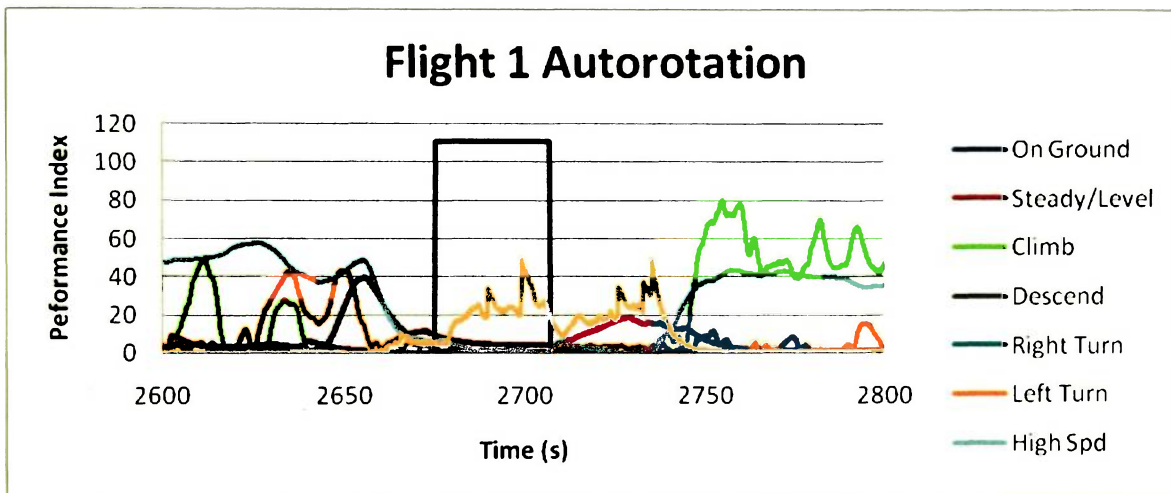


Figure 13: Autorotation Identification

The FRR algorithm can clearly identify when the rotorcraft is on the ground using the WOW value. The additional regimes identified with On Ground indicate combination maneuvers. Post processing analysis that looks at snapshots of data can more clearly identify On Ground combination maneuvers. Figure 11 shows a typical On Ground condition during the engine run up at the beginning of the flight. The high-speed entry into the on ground condition identified in Figure 12 can indicate a running landing. During the on ground portion, the rotorcraft transitions to a lower speed as indicated on the graph. The Autorotation, shown in Figure 13, can be identified by the high-speed descent that occurs just before the transition to on ground. Although this was a full-down autorotation, the rotorcraft did not remain on ground for long as indicated by the low speed level condition identified after the on ground condition.

5.2.2 High Speed

A large value for Indicated Airspeed (IAS) identifies that the rotorcraft is in a High Speed condition. The performance index for high-speed flight is proportional to the value for IAS. While High Speed is the dominant regime, the other regimes identified indicate combination maneuvers. The data below represents a typical High Speed identification. Figure 14 is a graph of the 600 to 900 second time interval of Flight 1. This selection contains High Speed, Climb, and Level Flight data. The input parameter and output regime values are from time step 720.4.

$$z_k = \begin{bmatrix} 13.62287 \\ 0 \\ 0.306887 \\ 45.6194 \\ 0 \\ -3.62625 \\ 0 \\ 3.739877 \end{bmatrix} \quad \hat{x}_k = \begin{bmatrix} 0 \\ 6.756455 \\ 11.83095 \\ 0.148182 \\ 1.52 \times 10^{-66} \\ 4.739045 \\ 56.52585 \\ 0.343349 \end{bmatrix}$$

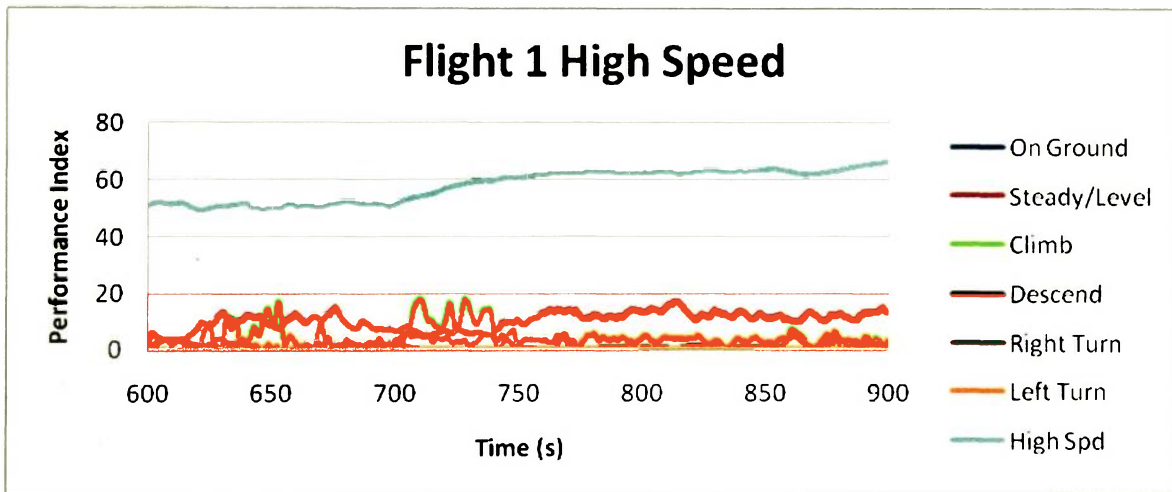


Figure 14: High Speed Identification

Figure 14 shows two High Speed combination maneuvers. High-speed climb occurs during two time intervals, 615 to 650 seconds and 700 to 750 seconds. An increasing vertical velocity causes the Climb regime identification. The second combination maneuver is High Speed Level flight. The level flight performance index is inversely proportional to the value for

altitude rate. Level flight is indicated during the first climb on Figure 14 because it is a steady climb with a low value for altitude rate and increasing vertical velocity.

5.2.3 Low Speed

A small value for IAS identifies that the rotorcraft is in a Low Speed condition. The performance index for low speed flight is inversely proportional to the value for IAS. While Low Speed is the dominant regime, the other regimes identified indicate combination maneuvers. The data below represents a typical Low Speed identification. Figure 15 is a graph of the 1800 to 2100 second time interval of Flight 2. This selection contains Low Speed Level Flight data. The input parameter and output regime values are from time step 1962.

$$z_k = \begin{bmatrix} 0 \\ 0 \\ 7.561601 \\ -1.851846 \\ -0.00459 \\ -2.5469 \\ 0 \\ 17.96111 \end{bmatrix} \quad \hat{x}_k = \begin{bmatrix} 0 \\ 17.71343 \\ 0.169022 \\ 0.22015 \\ 1.44 \times 10^{-23} \\ 3.079897 \\ 1.697266 \\ 39.01071 \end{bmatrix}$$

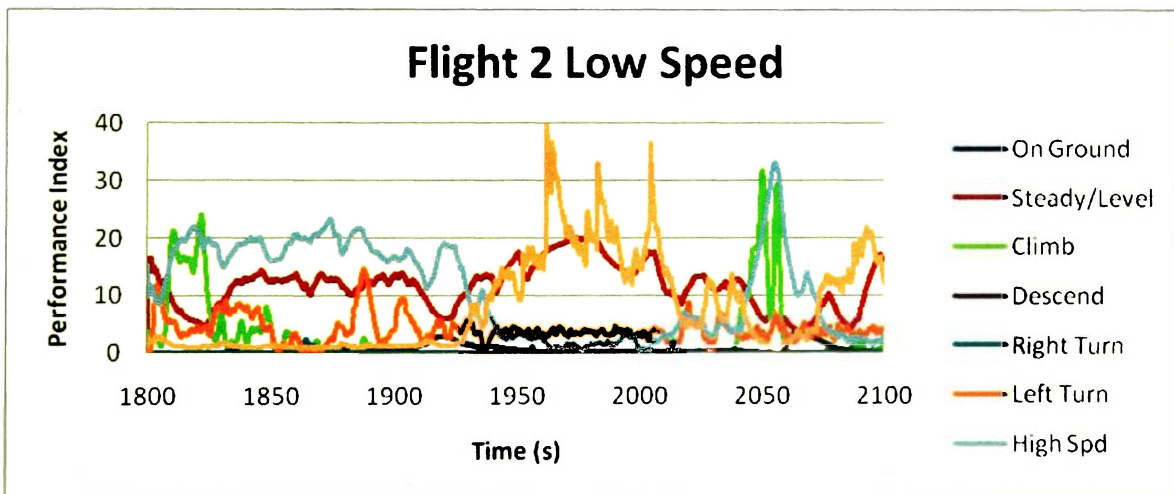


Figure 15: Low Speed Identification

Figure 15 demonstrates the FRR for the Low Speed regime, with an additional identification of Level flight. Low-speed flight was difficult to separate from high-speed flight

because both regimes rely on IAS for recognition. Ultimately, input scaling was necessary to ensure that the FRR Kalman filter identified low-speed flight at the proper time. Figure 15 clearly shows a transition between high-speed and low-speed flight, which demonstrates that the FRR algorithm can differentiate between the two conditions.

5.2.4 Right Turn

A large positive value for bank angle identifies that the rotorcraft is in a right turn. The performance index for Right Turn is proportional to the value for bank angle. While Right Turn is the dominant regime, the other regimes identified indicate combination maneuvers. The data below represents a typical Right Turn identification. Figure 16 is a graph of the 1500 to 1800 second time interval of Flight 3. This selection contains Right Turn, High Speed, Climb, and Descent data. The input parameter and output regime values are from time step 1764.

$$z_k = \begin{bmatrix} 0 \\ 0 \\ 0.300701 \\ 46.55785 \\ -14.5768 \\ 0 \\ 24.2862 \\ 0.686023 \end{bmatrix} \quad \hat{x}_k = \begin{bmatrix} 0 \\ 1.137711 \\ 9.47 \times 10^{-13} \\ 13.98413 \\ 30.27252 \\ 2.42 \times 10^{-25} \\ 54.82202 \\ 0 \end{bmatrix}$$

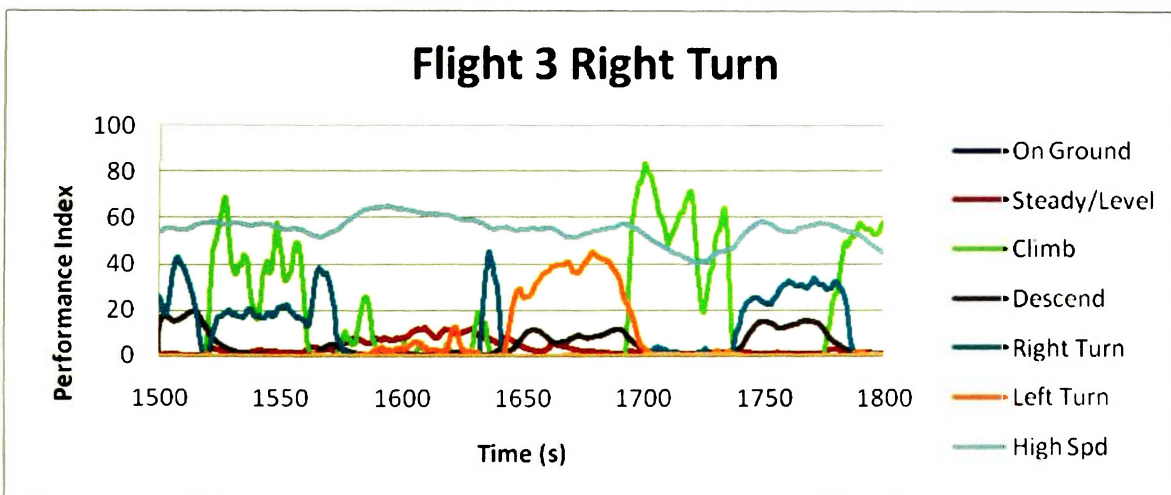


Figure 16: Right Turn Identification

Figure 16 demonstrates the regime recognition for Right Turn. The right turn condition identified by the filter is proportional to the value of bank angle. This means that the turns identified by the filter are banked turns, not pedal turns. The banked turns performed for the flight test included S-Turns that are indicated by a right-left-right or left-right-left turn pattern.

5.2.5 Left Turn

A large negative value for bank angle identifies that the rotorcraft is in a left turn. The performance index for Left Turn is proportional to the value for bank angle. While Left Turn is the dominant regime, the other regimes identified indicate combination maneuvers. The data below represents a typical Left Turn identification. Figure 17 is a graph of the 900 to 1200 second time interval of Flight 3. This selection contains Left Turn, High Speed, and Climb data. The input parameter and output regime values are from time step 1139.

$$z_k = \begin{bmatrix} 0 \\ 0 \\ 0.279334 \\ 50.11919 \\ 0 \\ -23.3389 \\ 0 \\ 2.979472 \end{bmatrix} \quad \hat{x}_k = \begin{bmatrix} 0 \\ 3.869957 \\ 0.000101 \\ 3.25804 \\ 7 \times 10^{-114} \\ 29.75149 \\ 62.27184 \\ 0.312022 \end{bmatrix}$$

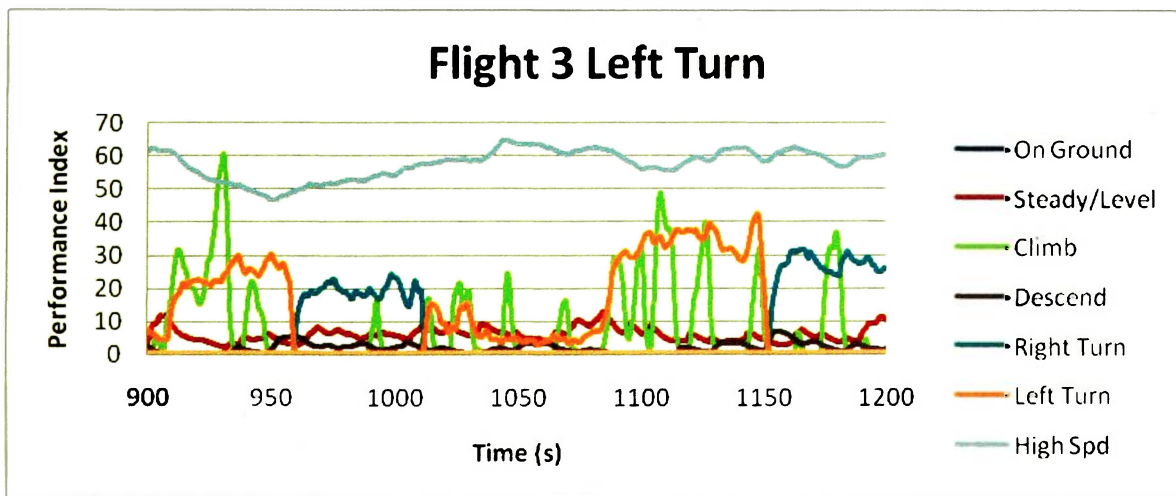


Figure 17: Left Turn Identification

Figure 17 demonstrates the regime recognition for Left Turn. The left turn condition identified by the filter is proportional to the value of bank angle. Figure 17 includes a snapshot of a left-right-left S-Turn from 900 to 1050 seconds. Post processing analysis of the FRR output data is required to identify this type of combination maneuver. Additionally, banked turns are relatively quick maneuvers identified for short time steps, as seen in Figure 17.

5.2.6 Climb

A large value for vertical velocity identifies that the rotorcraft is in a climb. The performance index for Climb is proportional to the value for vertical velocity. While Climb is the dominant regime, the other regimes identified indicate combination maneuvers. The data below represents a typical Climb identification. Figure 18 is a graph of the 300 to 600 second time interval of Flight 1. This selection contains Climb and High Speed data. The input parameter and output regime values are from time step 351.5.

$$z_k = \begin{bmatrix} 39.65059 \\ 0 \\ 0.386919 \\ 36.18329 \\ 0 \\ -3.5655 \\ 0 \\ 1.560516 \end{bmatrix} \quad \hat{x}_k = \begin{bmatrix} 0 \\ 1.863866 \\ 38.72848 \\ 0.002411 \\ 1.16 \times 10^{-37} \\ 4.1383 \\ 45.6639 \\ 0.425587 \end{bmatrix}$$

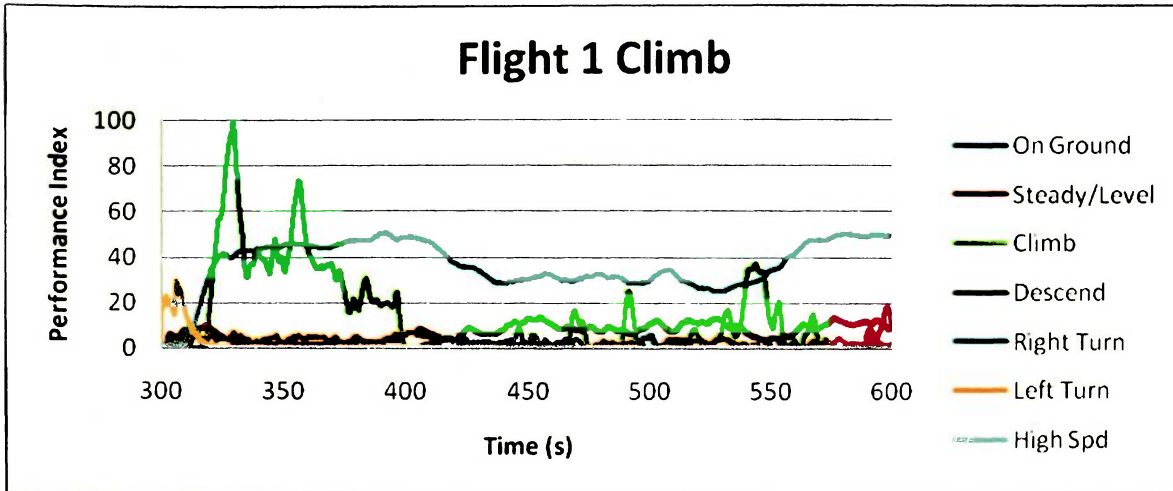


Figure 18: Climb Identification

Figure 18 clearly indicates a high-speed climb as the regime identified during the 315 to 400 second time interval. The performance indices for High Speed and Climb are the highest, and the other regimes all have values near zero during this time interval. The graph also shows a short duration high-speed climb around 550 seconds. Short duration climbs were performed during the flight tests. Short duration climbs helped the pilot maintain a safe altitude or to set-up for the next maneuver.

5.2.7 Descend

A large negative value for Rate of Climb (ROC) identifies that the rotorcraft is in a descent. The performance index for Descend is proportional to the value for ROC. While Descend is the dominant regime, the other regimes identified indicate combination maneuvers. The data below represents a typical Descend identification. Figure 19 is a graph of the 2400 to 2700 second time interval of Flight 1. This selection contains Descend, High Speed, and On Ground data. The input parameter and output regime values are from time step 2657.

$$z_k = \begin{bmatrix} 0 \\ 0 \\ 0.587424 \\ 23.83289 \\ -24.6594 \\ -2.62142 \\ 0 \\ 0.405524 \end{bmatrix} \quad \hat{x}_k = \begin{bmatrix} 0 \\ 1.033403 \\ 1.54 \times 10^{-8} \\ 37.60557 \\ 1.19 \times 10^{-36} \\ 5.827417 \\ 45.17738 \\ 0.443472 \end{bmatrix}$$

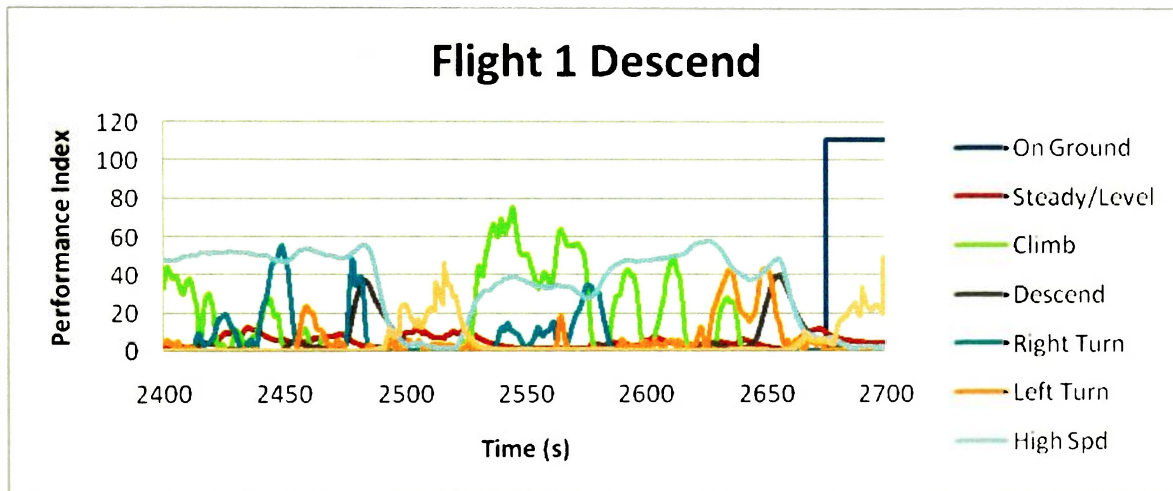


Figure 19: Descend Identification

The high-speed descent shown in Figure 19 prior to landing indicates an Autorotation. The graph also shows a high-speed right descending turn from 2470 to 2500 seconds. Descents identified by the FRR algorithm are typically short duration maneuvers. Short duration descents were performed during the flight test program. The short duration descents helped the pilot fly safely or to end the test maneuver performed.

5.2.8 Steady/Level Flight

A small value for ROC identifies that the rotorcraft is in Steady or Level Flight. The performance index for Steady/Level Flight is inversely proportional to the value for ROC. While Steady/Level Flight is the dominant regime, the other regimes identified indicate a combination maneuver. The data below represents a typical Steady/Level Flight identification. Figure 20 is a graph of the 1800 to 2100 second time interval of Flight 2. This selection contains Steady/Level

Flight, Low Speed, and High Speed data. The input parameter and output regime values are from time step 1970.

$$z_k = \begin{bmatrix} 0 \\ 0 \\ 6.022114 \\ 2.324765 \\ -0.10499 \\ -2.59208 \\ 0 \\ 18.86139 \end{bmatrix} \quad \hat{x}_k = \begin{bmatrix} 0 \\ 19.35844 \\ 0.029217 \\ 0.201222 \\ 9.89 \times 10^{-31} \\ 3.199035 \\ 1.414725 \\ 20.60146 \end{bmatrix}$$

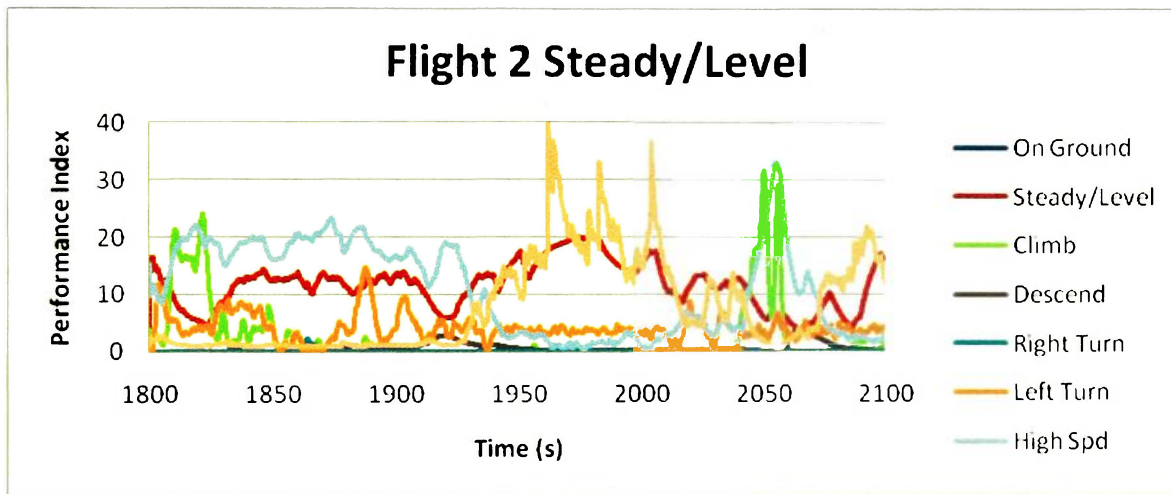


Figure 20: Steady/Level Flight Identification

Steady Flight is typically hover or a climbing maneuver, while Level Flight is typically a speed-based maneuver. The data examples provided throughout Section 5.2 demonstrate that Steady/Level is rarely identified as the dominant flight regime. This is a difficult flight regime to identify without additional data. It is currently impossible for the FRR algorithm to distinguish between the steady flight and level flight conditions. Post processing analysis can help determine if a steady flight or level flight condition existed. This type of post processing analysis relies upon user experience and practical flight knowledge.

5.3 Post Processing Regime Transition Identification

Regime transition identification focuses on the observation of the FRR for snapshots of the entire flight. The FRR algorithm generates an Excel file of the performance index values upon completion of a flight. Graphing these performance indices allows the user to observe the FRR for the entire flight. Regime transition identification requires graphs showing snapshots of a flight. The following figure represents a snapshot of regime transitions.

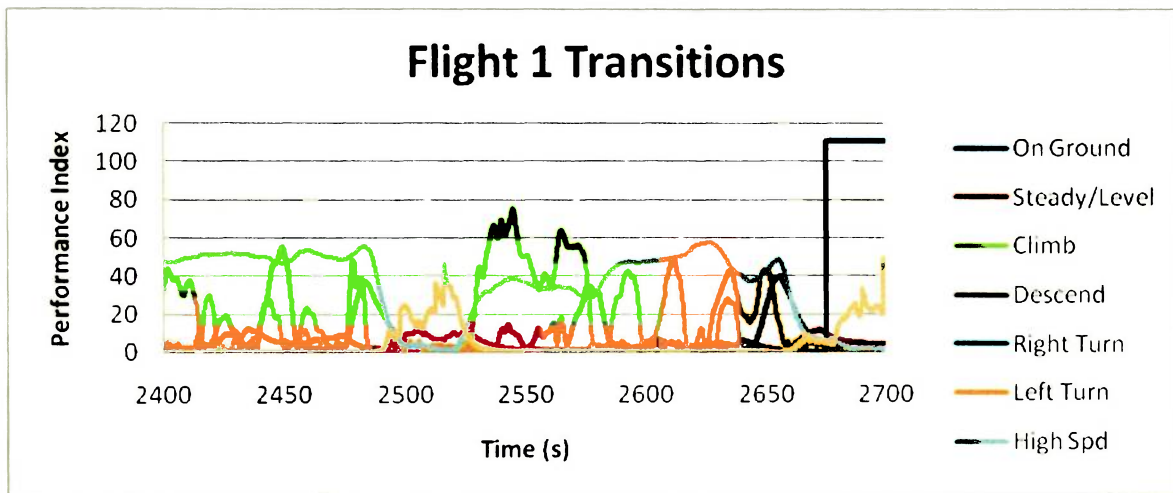


Figure 21: Regime Transitions

Figure 21 is a snapshot of Flight 1 during the 2400 to 2700 second time interval. Each of the eight regimes identified by the FRR Kalman filter appears on the graph. Additionally, seven of the eight regimes are clearly identified as a dominant regime on the graph. The graph begins with the rotorcraft in a high-speed climb. The aircraft then begins a right-left-right turning pattern. The final right turn of the pattern is a decelerating descending right turn. At approximately 2470 seconds, the rotorcraft transitions from high-speed to low-speed flight. The low-speed flight is relatively level. The aircraft then begins a high-speed climb with some slight right turning. At approximately 2650 seconds, the aircraft transitions to a high-speed descending left turn prior to landing. This final pattern indicates a left turn full-down autorotation. The maneuvers identified by this data snapshot were all performed as part of Flight 1. Figure 10 shows that the FRR algorithm appears to capture regime transitions appropriately for an entire flight.

5.4 Variation of Process Noise

Another application of post processing FRR analysis demonstrates the affect of varying process noise on the regime transition identification. Process noise accounts for uncertainty in the regime estimation based on the equations used to model the system. This is particularly useful to allow the filter to handle short duration parameter variations, such as from a gust of wind. Figure 21 shows the regime transitions for a process noise value of 0.001, which is the Q_k value used to obtain results for this thesis. The following figures show the affect of changing the process noise value on the regime identification. The data snapshots are from the 2400 to 2700 second time interval for Flight 1.

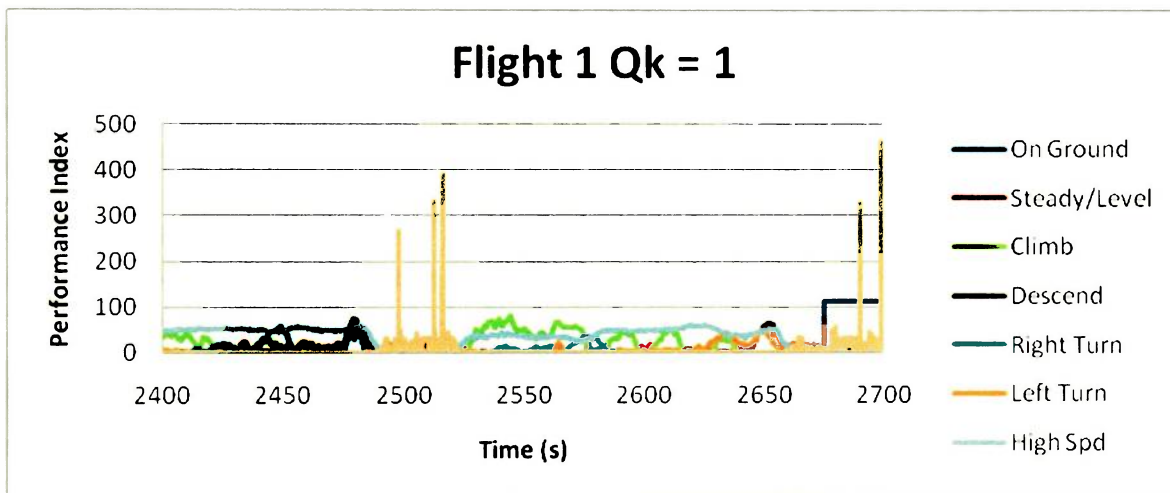


Figure 22: Regime Transitions with $Q_k = 1$

Figure 22 shows the FRR with a process noise value of 1. The Kalman filter still identifies regime transitions. The On Ground and High Speed regime identification appears mostly unchanged with the increased noise. The Low Speed regime is identified as the dominant regime more often, but there are large spikes in this regime's recognition. The short duration large jumps in Low Speed indicate a misidentification or out of bounds value at those time intervals. These inaccurate Low Speed performance indices represent noise which the filter is using as valid data. The large process noise value seems to better identify the Right Turn, Left Turn, Climb, and Descend regimes without creating misidentification or out of bounds values. Additional scaling or saturation are required on the Low Speed input parameter to utilize this higher process noise value.

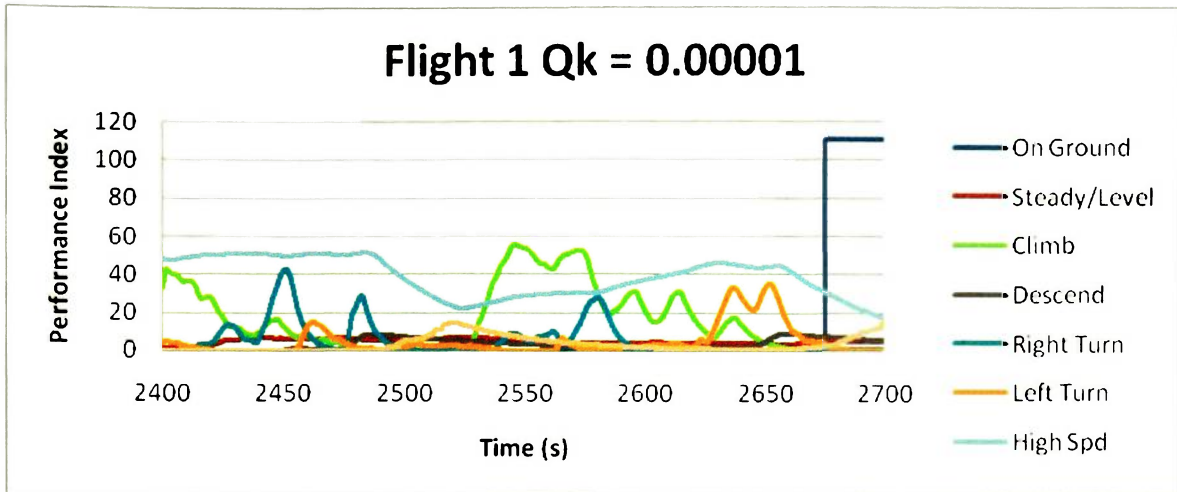


Figure 23: Regime Transitions with $Q_k = 0.00001$

Figure 23 shows the FRR with a process noise value of 0.00001. The Kalman filter still identifies regime transitions, but much of the valid data is ignored by the filter. The Low Speed, Level Flight, and Descend regimes are barely identified. The High Speed, Climb, Right Turn, and Left Turn regimes are identified but the performance indices are severely degraded by the lower noise threshold. A process noise value of 0.00001 is simply unfit for this FRR algorithm. However, the process noise values displayed in Figure 22 and Figure 23 can help develop a noise band which is acceptable for the FRR Kalman filter.

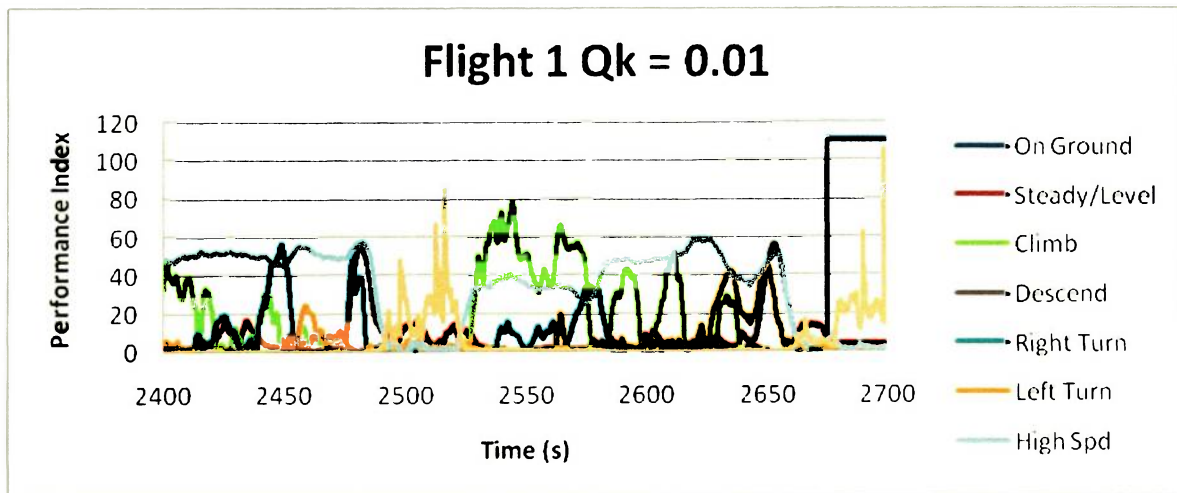


Figure 24: Regime Transitions with $Q_k = 0.01$

Figure 24 shows an acceptable value for process noise in the FRR algorithm developed for this thesis. The Low Speed and Descend regimes are more clearly identified by raising the

acceptable noise threshold. The High Speed, On Ground, Climb, Right Turn, and Left Turn regimes appear unaffected by the change in process noise. This represents a higher process noise value than was used for the analysis herein, but is an acceptable upper bound for the process noise band in the FRR Kalman filter.

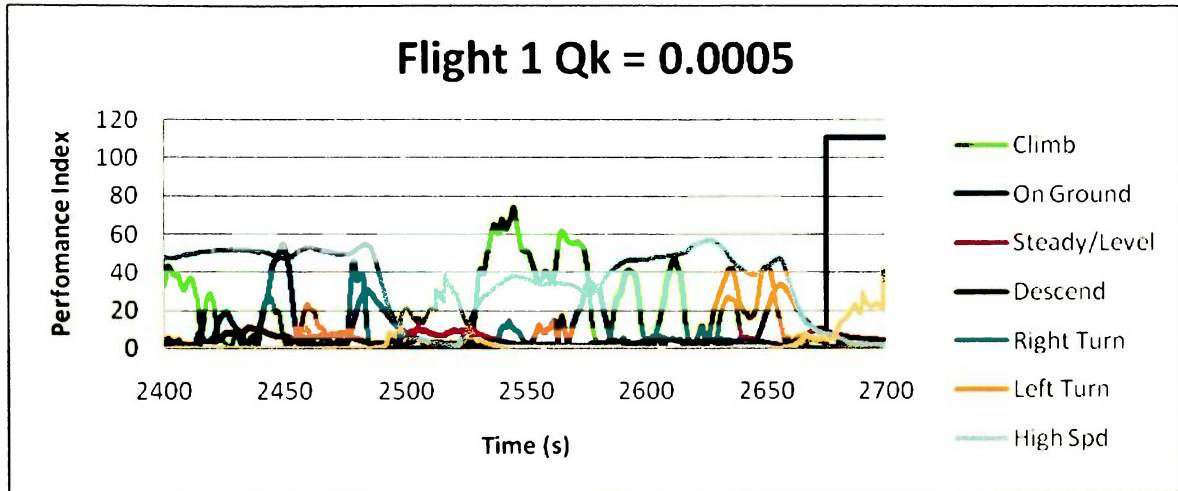


Figure 25: Regime Identification with $Q_k = 0.0005$

Figure 25 shows an acceptable value for process noise in the FRR algorithm developed for this thesis. The regimes are still identified with acceptable accuracy. The Low Speed and Descend regimes are still identified, even though the acceptable noise threshold is lower. The High Speed and On Ground regimes appear relatively unaffected by the change in process noise. The Climb, Right Turn, and Left Turn regimes are affected by the change but remain properly identified. The Level Flight regime identification is difficult with the lower process noise value, thus a better identifying parameter would be required if this noise threshold was used. The process noise value shown in Figure 25 represents a lower bound for the process noise band of the FRR Kalman filter.

The figures above demonstrate the affect of varying process noise on the FRR performed by the Kalman filter developed for this study. The acceptable process noise band, shown in Figure 24 and Figure 25, is $Q_k = 0.01 \rightarrow 0.0005$. As the process noise value is increased the filter relies on more of the input data to determine the performance index estimates. This allows short duration parameter jumps to affect the regime performance indices. This also creates a possibility for short duration regime transitions to be identified by

the FRR algorithm. More regime transition points are captured by increasing the process noise value, but these may not necessarily be actual regime transitions.

As the process noise value is decreased the filter relies more on the state model and less on the input data [13]. Recall that the State Transition Matrix, Φ_k , is an identity matrix. This tells the filter to estimate the performance index at the next time step to be the same as the current time step based on the Kalman filter equation, $\hat{x}_k = \Phi_k \hat{x}_{k-1} + w_k$. When the process noise value is low and less input data is used to estimate the performance indices, the filter uses more of the previous performance index estimate to determine the current regime. This creates a possibility for valid data to be ignored by the filter and degrades the regime identification. Fewer regime transition points are identified by decreasing the process noise value. Actual regime transition points may be missed by the filter if the process noise value is too low.

6. CONCLUSIONS

This study uses a Kalman filter to perform real-time FRR analysis. The Kalman filtering approach provided herein performs FRR to identify when the rotorcraft is in the flight regimes listed in Appendix A. The recorded flight parameters, listed in Appendix B, allow the Kalman filter to identify the flight regimes. The data used in this study was gathered during the ERAU HUMS Schweizer 300 Flight Test Program. The ERAU HUMS team used the Kalman filter developed during this thesis for FRR analysis. The use of a Kalman filter to perform FRR appears to be a new application of Kalman filtering.

The FRR algorithm detailed herein has been successful in performing real-time FRR analysis. A real-time graphical display shows the performance index values and allows the user to observe regime transitions. Recorded flight parameters determine the performance index values. Each parameter corresponds to one and only one regime. This ensures that the performance index value for one regime is not dependent on the value for another regime. The independent calculation of the performance indices was used to prove that the FRR algorithm developed herein works properly. Future work with this FRR algorithm may utilize dependent regimes to expand the number of regimes identified. Typically, it is preferable to identify a regime using several flight parameters. Future work with this FRR algorithm should enable the Kalman filter to identify a regime using multiple parameters.

The FRR algorithm developed herein identifies eight major flight regimes using eight flight parameters. The algorithm also indicates combination maneuvers which the user verifies via the real-time graphical display or post processing graphical analysis. Transitions between flight regimes are observable both on the real-time display and post processing results. Regime identification and regime transition points are dependent upon the process noise values. An acceptable process noise band presented for this FRR algorithm is $Q_k = 0.01 \rightarrow 0.0005$. Future work with this algorithm to add regimes or include dependent regimes may require a different process noise band.

The Kalman filter is the basis of the FRR algorithm described herein. The filter is readily accessible and modifiable within the MATLAB code. This accessibility is a major benefit of

Kalman filtering. Another benefit is the inherent handling of noise. The measurement noise, or signal variance, filter input is the OEM listed sensitivity value for each sensor. In addition to measurement noise, the filter treats process noise. Mathematically process noise is the uncertainty in the state estimate due to equation error. Physically process noise allows the filter to account for short duration jumps in the input parameter values. This ensures that a gust of wind will not cause the filter to misidentify the regime or change regimes for a short duration.

Another benefit of the Kalman filter is that it can utilize a priori and a posteriori information. The FRR application described herein does not have a priori information because there is no information about what regime the rotorcraft is in prior to entering that regime. However, a posteriori information can be utilized by feeding back the state estimates. This would enable a regime to be identified only after another regime has been entered. For example, a takeoff will only be identifiable if the rotorcraft has previously been on the ground. The simple regime identification demonstrated in this paper does not use state feedback, but it would be relatively easy to add to this filter.

Many HUMS applications require real-time or post-processing analysis of FRR results. These applications include conditioned based maintenance and actual flight spectrum analysis. The post processing analysis results described herein show that the application of a Kalman filter for a real-time FRR algorithm has been successful. The real-time graphical display developed herein is user friendly and allows the user to observe regime identification and transitions.

7. REFERENCES

[1] Le, Dy. "The Federal Aviation Administration: Rotorcraft Structural Integrity and Safety." <<http://aar400.tc.faa.gov/Programs/agingaircraft/rotorcraft/index.htm>> Updated: August 15, 2006. Accessed: November 13, 2007.

[2] Le, Dy. "The Federal Aviation Administration: Health and Usage Monitoring Systems (HUMS)." <<http://aar400.tc.faa.gov/Programs/agingaircraft/rotorcraft/index.htm>> Updated: August 14, 2006. Accessed: November 13, 2007.

[3] Klein, Vladislav, and Eugene A. Morelli. Aircraft System Identification: Theory and Practice. AIAA Education Series. American Institute of Aeronautics and Astronautics, 2006.

[4] Ganguli, Ranjan, Iderjit Chopra, and David J. Haas. "Helicopter Rotor System Fault Detection Using Physics-Based Model and Neural Networks." *AIAA Journal*. Vol. 36, No. 6. American Institute of Aeronautics and Astronautics. 1998, pp.1078-1086.

[5] Ganguli, Ranjan. "Health Monitoring of a Helicopter Rotor in Forward Flight Using Fuzzy Logic." *AIAA Journal*. Vol. 40, No. 12. American Institute of Aeronautics and Astronautics. 2002, pp. 2373-2381.

[6] Alkahe, Jonathan, Yaakov Oshman, and Omri Rand. "Adaptive Estimation Methodology for Helicopter Blade Structural Damage Detection." *Journal of Guidance, Control, and Dynamics*. Vol. 25, No. 6. American Institute of Aeronautics and Astronautics. 2002, pp. 1049-1057.

[7] McCool, Kelly and Gene Barndt. "Assessment of Helicopter Structural Usage Monitoring System Requirements." *DOT/FAA/AR-04/3*. April 2004.

[8] Dickson, B., J. Cronkhite, S. Bielefeld, L. Killian, and R. Hayden. "Feasibility Study of a Rotorcraft Health and Usage Monitoring System (HUMS) Usage and Structural Life Monitoring Evaluation." *DOT/FAA/AR-95/9. ARL-CR-209. NASA CR-198447*. February 1996.

[9] Augustin, Michael. "Hazard Assessment for Usage Credits on Helicopters Using Health and Usage Monitoring System." *DOT/FAA/AR-04/19*. July 2004.

[10] Michael, James, Geoffrey Collingwood, Michael Augustin, and James Cronkhite. "Continued Evaluation and Spectrum Development of a Health and Usage Monitoring System." *DOT/FAA/AR-04/6*. May 2004.

[11] He, Dr. David, Shenliang Wu, and Dr. Eric Bechhoefer. "Development of Regime Recognition Tools for Usage Monitoring." IEEE Aerospace Conference. 3-10 March 2007. Big Sky, MT. pp 1-11.

[12] Wu, Shenliang, Dr. Eric Bechhoefer, and Dr. David He. "A Practical Regime Prediction Approach for HUMS Applications." American Helicopter Society Annual Forum. 1-3 May 2007. Virginia Beach, VA. Conference 63. Vol. 2. pp 1440-1447.

[13] Musoff, Howard, and Paul Zarchan. Fundamentals of Kalman Filtering: a Practical Approach. 2nd ed. Vol. 208. AIAA Progress in Astronautics and Aeronautics Series. Reston, VA: American Institute of Aeronautics and Astronautics, 2005.

[14] Anderson, Dr. Richard P., Dr. Andrew Kornecki, Dr. Nikolas D. Macchiarella, et al. Installation of the Structural Integrity Monitoring System for Usage Credits on the Schweizer 300. Intermediate Report. Embry-Riddle Aeronautical University and Federal Aviation Administration. Daytona Beach, FL. April 2008.

8. APPENDIX A: IDENTIFIED REGIMES

| Regime |
|--------------|
| On Ground |
| Level Flight |
| Climb |
| Descend |
| Left Turn |
| Right Turn |
| High Speed |
| Low Speed |

9. APPENDIX B: FLIGHT PARAMETERS

| Paramter | Eng Units |
|-------------------------------|-----------|
| WOW | 0, 100 |
| ROC (EII Alt) negative | ft/min |
| IAS | kts |
| w positive | ft/s |
| ϕ positive | deg |
| ϕ negative | deg |
| Inv (IAS) | s/ft |
| inv (ROC(EII Alt)) (0-100fpm) | min/ft |